Available online at www.sciencedirect.com
ScienceDirect
Journal of Computational Physics 223 (2007) 316–340
JOURNAL OF COMPUTATIONAL PHYSICS
www.elsevier.com/locate/jcp

Grid stabilization of high-order one-sided differencing I: First-order hyperbolic systems

Thomas Hagstrom [a,*], George Hagstrom [b]

[a] Department of Mathematics and Statistics, The University of New Mexico, Albuquerque, NM 87131, United States
[b] Department of Physics, University of Texas at Austin, Austin, TX, 78712, United States

Received 3 December 2005; received in revised form 5 August 2006; accepted 12 September 2006
Available online 13 November 2006

Abstract

We construct stable, maximal order boundary closures for high order central difference methods. The stability is achieved by adding a small number of additional subcell nodes near the boundaries at experimentally determined locations. We find that methods up through 8th order can be stabilized by the addition of a single node, up through 16th order by the addition of two nodes, and up through 22nd order with three extra nodes. We also consider the application of the technique to dispersion relation preserving methods, and we construct and test artificial dissipation operators.

Keywords: One-sided differencing; Hyperbolic systems; Stability

1. Introduction

Simple analysis and computational experience both suggest that high order or, more generally, high resolution methods are required for the efficient solution of problems which involve wave propagation over many wavelengths. Therefore, high order methods using both structured (e.g. [15]) and unstructured (e.g. [11]) grids have been extensively studied. A potential advantage of structured grid approaches is the weak dependence on method order of the time step stability constraints of the standard central difference approximations. However, it has been difficult to construct stable boundary closures, which match the order of the interior schemes.

In [18], a systematic procedure for building stable boundary closures is given. The idea is to construct boundary closures and modified inner products such that a discrete summation-by-parts formula holds, and thus they are referred to as SBP methods. In [16,17,3] and elsewhere techniques are proposed to exploit this property to derive stable, fully discrete approximations. However, a defect of these methods, particularly if the more convenient diagonal norms are to be used [19], is that the order of the boundary closures may be limited relative to the order of the interior scheme; precisely only orders half those of the interior scheme can be constructed [18].

* Corresponding author. Tel.: +1 505 277 8920; fax: +1 505 277 5505.
E-mail addresses: hagstrom@math.unm.edu (T. Hagstrom), georgehagstrom@mail.utexas.edu (G. Hagstrom).

0021-9991/$ - see front matter
doi:10.1016/j.jcp.2006.09.017

In this work, we pursue an alternative approach which apparently avoids the order restrictions mentioned above and which allows a completely straightforward derivation of the difference formulas. Our premise is that the instability of the maximal order one-sided difference formulas is simply a manifestation of the Runge phenomenon. Therefore, we seek to counteract it by refining the grid near the boundary. Precisely, we insert a small number of additional nodes (1–3) in the first or first two cells. We note that a boundary refinement strategy obviously works in the extreme limit of pseudospectral approximations [5], though then a considerable fraction of the grid must be concentrated near the edges. In [7], we developed stable methods using the hybrid Gauss-Trapezoid quadrature nodes constructed in [1]. However, it is clear that such precise node locations are not necessary to obtain stability. Here we attempt to find the minimal number of additional nodes required to produce stable closures. We find experimentally that only one additional node is needed for methods of order 8 and below, that only two additional nodes are needed for methods of order 16 and below, and that with three additional nodes we can stabilize methods up to order 22.

The remainder of the paper is organized as follows. In Section 2, we describe in detail our grid construction, which involves minimizing the spectral radius of the difference operator with boundary conditions subject to the stability constraint on the sign of its eigenvalues. In Section 3, we further analyze the stability of the resulting boundary closures by examining the determinant condition associated with the Laplace transform of its semidiscretization. In Section 4, we extend our construction to Tam and Webb's DRP schemes [20] and in Section 5 we construct stable artificial dissipation operators. Numerical experiments with constant coefficient and variable coefficient linear systems are presented in Section 6. Finally, we conclude in Section 7 and suggest problems for future work.

2. Construction of the grids

Consider approximations to the first derivative, $\mathrm{d}/\mathrm{d}x$, for functions, u, defined on the interval $x \in [0,1]$ satisfying the boundary condition $u(1) = 0$. We introduce a grid, $\mathscr{G}_h$, which is the union of the uniform grid with mesh width $h = 1/N$ and a finite number of additional nodes:

$$\mathscr{G}_h = \{jh,\ 0 \leqslant j \leqslant N\} \bigcup \{z_k\, h, 1 - z_k h,\ k = 1, \ldots, p\}, \tag{2.1}$$

where $z_k \notin \mathbb{Z}$ (In what follows we will only consider $p = 1$, 2, 3 and $0 < z_k < 2$. That is, extra points will be located in the first two cells.). An approximate derivative operator, D_{2q}, of order $2q$ is defined in the following way. Let U be a function defined on $\mathscr{G}_h$. For nodes on the uniform grid whose q nearest neighbors to each side are also nodes on the uniform grid we take $(D_{2q}U)_j$ to be the standard $2q$th order central difference approximation as defined, for example, in [6, Chapter 3]:

$$D_{2q}U_j = \frac{1}{h}\sum_{k=1}^{q} \beta_k (U_{j+k} - U_{j-k}), \tag{2.2}$$

with the β_k being grid-independent coefficients. For the other nodes we simply use the derivative of the degree $2q$ interpolating polynomial constructed from the data at the target node and $2q$ neighbors: q taken from each side when possible and taken from the boundary node into the domain when not. The resulting operator can be represented as a banded matrix of dimension $(N + 2p + 1) \times (N + 2p + 1)$ identifying grid functions with vectors of length $(N + 2p + 1)$ and assuming the elements are ordered according to the order of the nodes. Lastly, we impose the boundary condition $U(1) = 0$ by eliminating the last row and column of this matrix, resulting in an $(N + 2p) \times (N + 2p)$ matrix, $\mathscr{D}_{2q,h}$.

Our criteria for grid construction are based on the spectra of the matrices $\mathscr{D}_{2q,h}$. A straightforward calculation shows that the continuous first derivative operator defined in an appropriate space of functions satisfying the boundary conditions in fact has no spectrum (Simply solve $\frac{\mathrm{d}u}{\mathrm{d}x} - \lambda u = F$, $u(1) = 0$ for arbitrary $\lambda \in \mathbb{C}$.). Thus *all* eigenvalues of $\mathscr{D}_{2q,h}$ are in some sense spurious. As our goal is to construct stable approximations to the well-posed hyperbolic initial boundary value problem:

$$u_t = u_x + F,\ u(x,0) = g(x),\ u(1,t) = 0, \tag{2.3}$$

we require a stable semidiscretization; that is we require that the eigenvalues of $\mathscr{D}_{2q,h}$ have negative real part. In addition, we wish to minimize the time step stability constraint. In detail this would require a specific choice for the time stepping scheme, so as a surrogate we minimize the spectral radius. Thus we approximately solve:

Problem 1. For fixed N, p, q choose $\{z_k, k = 1, \ldots, p\}$ to minimize $\rho(\mathscr{D}_{2q,h})$ subject to $\sigma(\mathscr{D}_{2q,h}) \subset \mathbb{C}^-$.

An obvious defect of the direct use of Problem 1 to choose a grid for a practical calculation is the probable N-dependence of the results. However, our experiments show that the N-dependence is weak for N large enough compared with p and q, so we will simply use approximate minimizers calculated for fixed values of N.

Of course it would be possible to employ minimization software to compute the optima. However, given the small number of parameters to be determined and the restrictions on their values we simply employed a brute force search, sampling z_j on a grid of width $\Delta z = 0.01$.

2.1. Results

We consider three possibilities: one extra point in the first cell, two extra points in the first cell, and three extra points – two in the first cell and one in the second (Putting three points in the first cell was ineffective.). In each case grids were found with feasible – that is stable – discretizations up to some maximum order. Beyond the maximum order no stable discretizations were found. The maximum orders for which grids were constructed in this way were 8 when $p = 1$, 16 when $p = 2$, and 22 when $p = 3$. We tabulate below the values of z_j which approximately solve the constrained problem along with basic properties of the spectrum for $N = 100$ and $N = 200$.

We note that if methods of a given order could be stabilized for a certain value of p then so could all methods of lower order. As indicated by the case $2q = 8$, $p = 2$, increasing p beyond the minimum value required for a given order tended to increase the spectral radius. However, for very high-order methods increasing p did produce more robustly stable approximations. This is discussed further in the section on numerical experiments, where we recommend the restriction $2q \leqslant 12$ for $p = 2$ and $2q \leqslant 18$ for $p = 3$. We see that the spectral radius itself, when scaled by the interior grid spacing, appears insensitive to N. However, the distance of the spectrum from the imaginary axis decreased as N increased. It is of interest to view plots of the spectra themselves (see Figs. 1–3.). We consider $2q = 8$ with $p = 1$, $2q = 16$ with $p = 2$, and $2q = 22$ with $p = 3$. In all cases the spectrum consists of a large number of eigenvalues lying on what appears to be a smooth curve plus a small number of outlying eigenvalues. The latter determine the spectral radius while the edge of the former usually determines the maximum real part (see Table 1).

Lastly, we note that once the z_k have been chosen, the coefficients of the difference methods are directly computed by constructing and differentiating the appropriate Lagrange polynomials. For ease of implementation we have simply performed this calculation at startup. For example at the left boundary if $x_1 < x_2 < \cdots < x_{2q+1}$ are the first $2q + 1$ nodes (including the extra nodes) and x_k is a node where the central difference formula is not employed we have the unbalanced formula:

$$(\mathscr{D}_{2q,h}U)_k = \frac{1}{h}\sum_{j=1}^{2q+1} \alpha_{kj} U_j \tag{2.4}$$

where we compute α_{kj} by introducing $\tilde{x} = \frac{x - x_1}{h}$, $\tilde{x}_j = \frac{x_j - x_1}{h}$ and computing the coefficients of the Lagrange polynomials:

$$L_j(\tilde{x}) = \prod_{k=1 k\neq j}^{2q+1} \frac{\tilde{x} - \tilde{x}_k}{\tilde{x}_j - \tilde{x}_k} \tag{2.5}$$

Then:

$$\alpha_{kj} = L_j'(\tilde{x}_k). \tag{2.6}$$

We could, however, tabulate the coefficients in each case for select choices of the extra nodes. In Eq. (A.37) in Appendix, we list in detail the 8th order one-sided approximations with $p = 1$ and $z_1 = \frac{1}{5}$ (We chose $\frac{1}{5}$ instead of the optimal value 0.19 to produce simpler rational coefficients.).

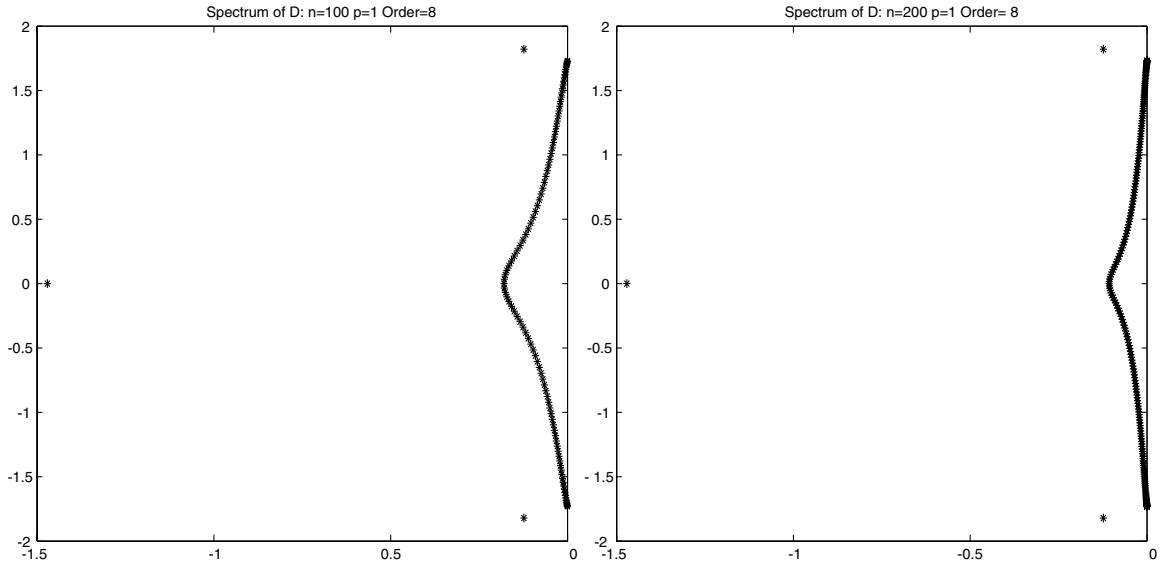

Fig. 1. Spectra of $h\mathscr{D}_{8,h}$ for $p = 1$.

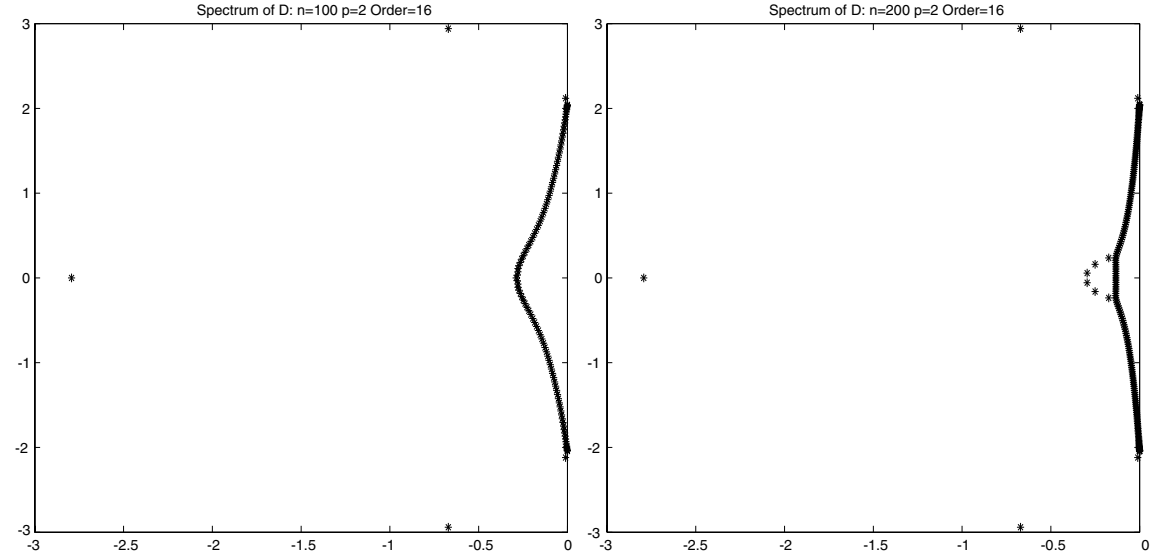

Fig. 2. Spectra of $h\mathscr{D}_{16,h}$ for $p = 2$.

2.2. Sensitivity

As the grid construction depends on an ad hoc numerical minimization with an arbitrary choice of the number of nodes in the interval, it is of interest to check the sensitivity of the important spectral quantities with respect to variations in the node locations and in the number of nodes. We present such studies below focusing on three cases: 8th order approximations with $p = 1$, 12th order approximations with $p = 2$, and 16th order approximations with $p = 2$.

For the first case, we consider varying the node location, z_1, between 0.05 and 0.35 with $N = 200$ fixed. The results, shown in Fig. 4, show that the discretization is stable for z_1 in a wide subinterval about the optimal value 0.19. The spectral radius, on the other hand, shows rapid growth as z_1 is decreased below the optimal

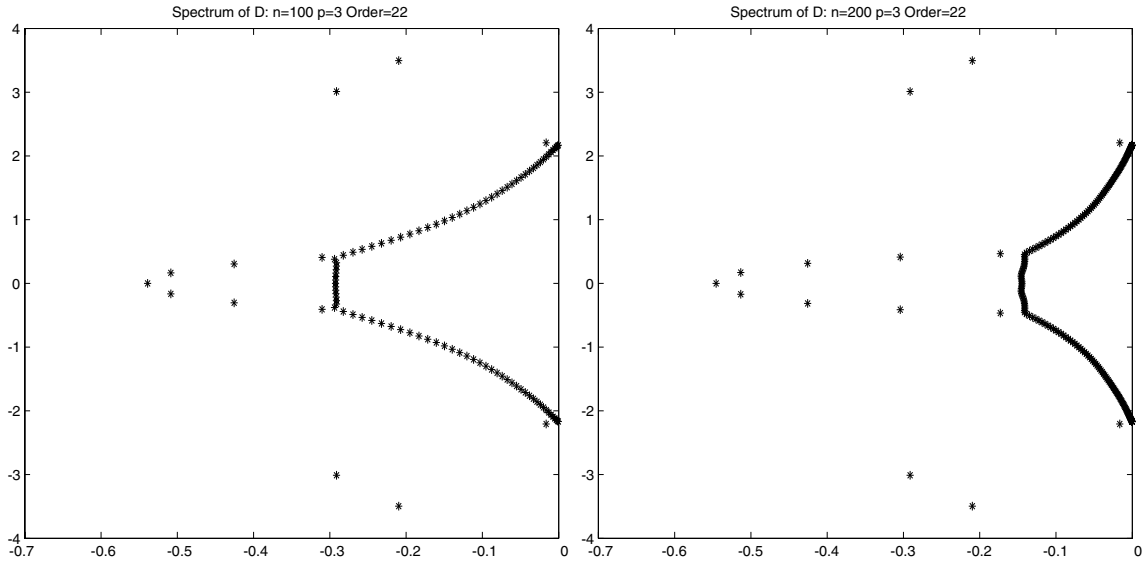

Fig. 3. Spectra of $h\mathscr{D}_{22,h}$ for $p = 3$.

Table 1
Optimized grid locations and spectra of $\mathscr{D}_{2q,h}$

z_1	z_2	z_3	$2q$	N	$N^{-1}\rho(\mathscr{D})$	$N^{-1}\max_{\lambda\in\sigma(\mathscr{D})}\Re\lambda$
0.89	–	–	4	100	1.65	−4.84(−5)
0.89	–	–	4	200	1.65	−5.79(−6)
0.21	–	–	6	100	1.59	−7.63(−5)
0.21	–	–	6	200	1.59	−9.09(−6)
0.19	–	–	8	100	1.83	−1.10(−4)
0.19	–	–	8	200	1.83	−1.25(−5)
0.13	0.83	–	8	100	3.02	−1.36(−4)
0.13	0.83	–	8	200	3.02	−1.62(−5)
0.13	0.97	–	10	100	3.05	−1.55(−4)
0.13	0.97	–	10	200	3.05	−1.82(−5)
0.13	0.87	–	12	100	2.95	−2.09(−4)
0.13	0.87	–	12	200	2.95	−2.40(−5)
0.10	0.53	–	14	100	3.05	−2.83(−4)
0.10	0.53	–	14	200	3.05	−3.03(−5)
0.10	0.53	–	16	100	3.02	−1.94(−4)
0.10	0.53	–	16	200	3.02	−1.94(−5)
0.10	0.43	1.90	18	100	3.45	−4.00(−4)
0.10	0.43	1.90	18	200	3.45	−4.30(−5)
0.10	0.43	1.86	20	100	3.40	−5.38(−4)
0.10	0.43	1.86	20	200	3.40	−5.44(−5)
0.10	0.43	1.77	22	100	3.50	−4.19(−4)
0.10	0.43	1.77	22	200	3.50	−3.90(−5)

value, but very slow growth as it is increased. Thus these basic properties of the spectrum are essentially unchanged for increasing z_1 beyond the optimal value 0.19 to about 0.31.

We now fix $z_1 = 0.19$ and vary N from 20 to 1000. As seen in Fig. 5, the scaled spectral radius is essentially constant. The maximum real part, on the other hand, does increase with increasing N more rapidly than a simple scaling by the mesh width.

Moving on to the cases with $p = 2$, we first consider 12th order methods, varying (z_1, z_2) in the rectangle $[0.05, 0.35] \times [0.4, 0.9]$ and fixing $N = 100$. The stability region as well as contour plots of the spectral radius are shown in Fig. 6. Again we find that the approximations are stable for a wide range of parameter values

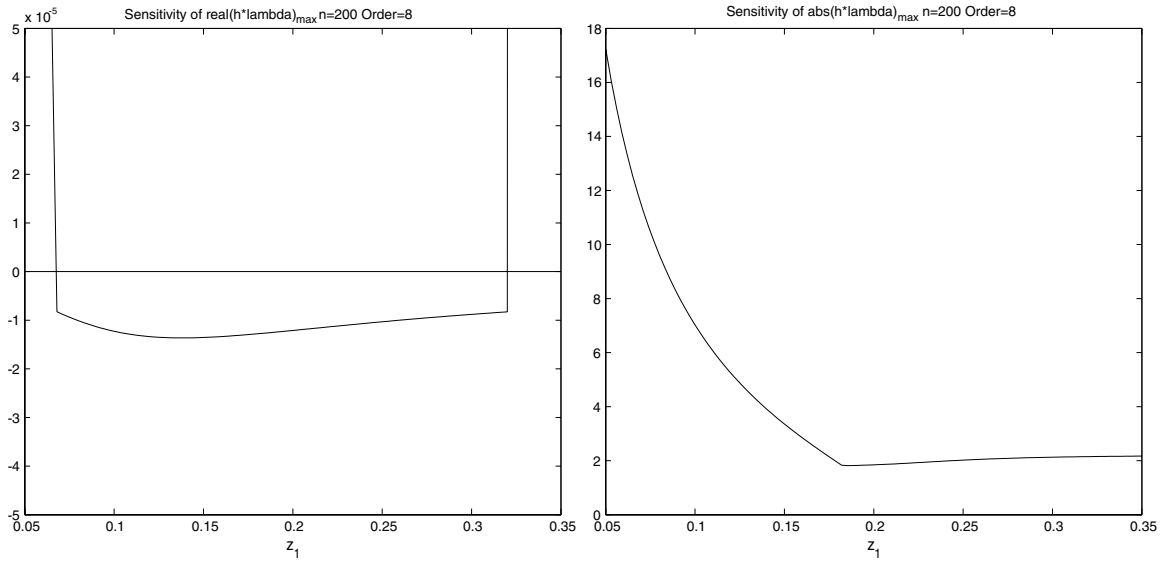

Fig. 4. Sensitivity of spectral quantities for $h\mathscr{D}_{8,h}$ with $p = 1$ and varying z_1.

and that the spectral radius is well-behaved so long as z_1 is not chosen too small. Fixing $z_1 = 0.10$ and $z_2 = 0.53$ we observe that the N-dependence of these quantities is similar to the case above except that the distance of the spectrum to the imaginary axis is about an order of magnitude greater than in the previous case (see Fig. 7).

Repeating the preceding experiment for 16th order discretizations we observe a smaller stability region displaced towards smaller values of z_j (Note the change of z-values plotted in Fig. 8.). Nonetheless, variations of more than 0.1 in each parameter are permitted. Similarly, the region where the spectral radius is small is obviously smaller. This indicates an increased sensitivity to the choice of grid parameters relative to the 12th order approximations. The response to variations of N, on the other hand, are essentially the same as for the lower order methods (see Fig. 9).

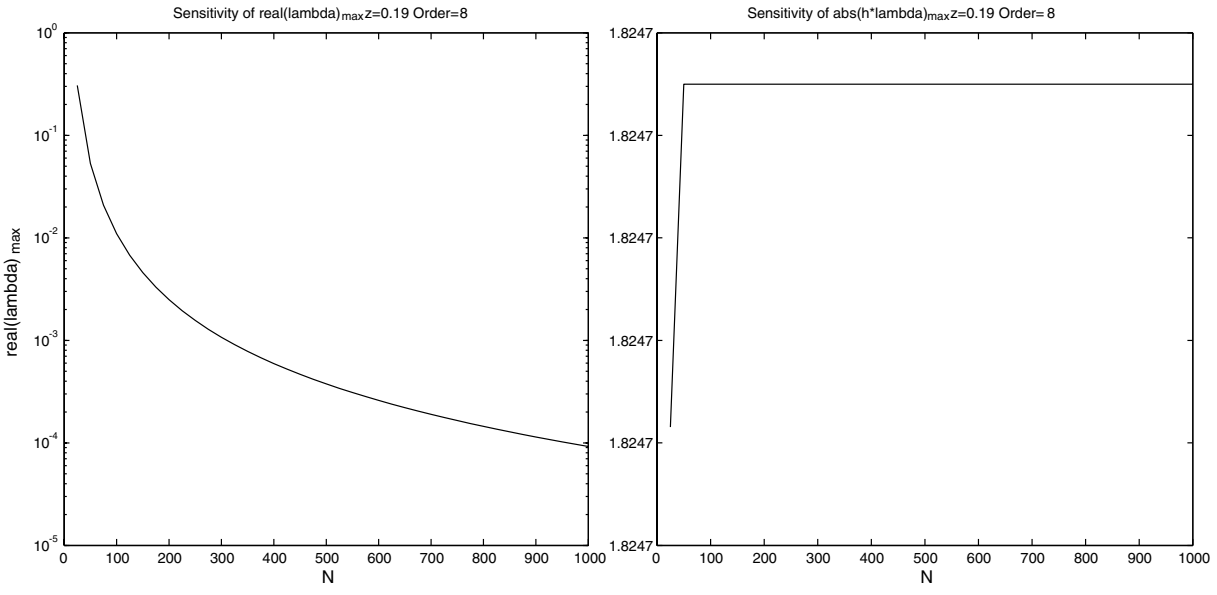

Fig. 5. Sensitivity of spectral quantities for $h\mathscr{D}_{8,h}$ with $p = 1$ and varying N.

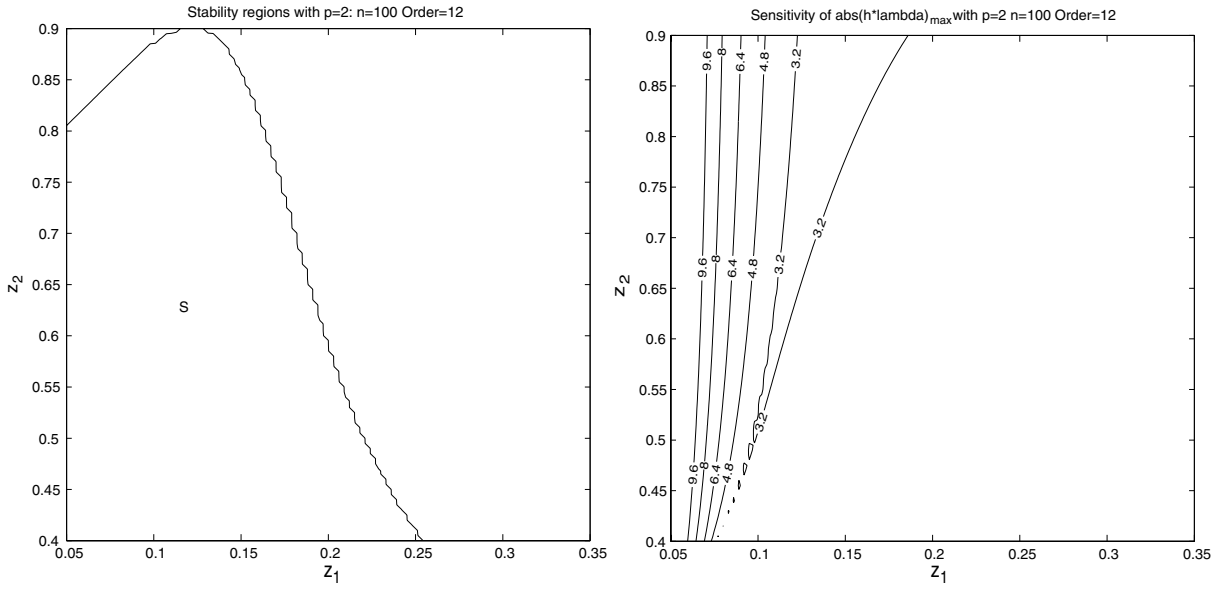

Fig. 6. Sensitivity of spectral quantities for $h\mathscr{D}_{12,h}$ with $p = 2$ and varying (z_1, z_2).

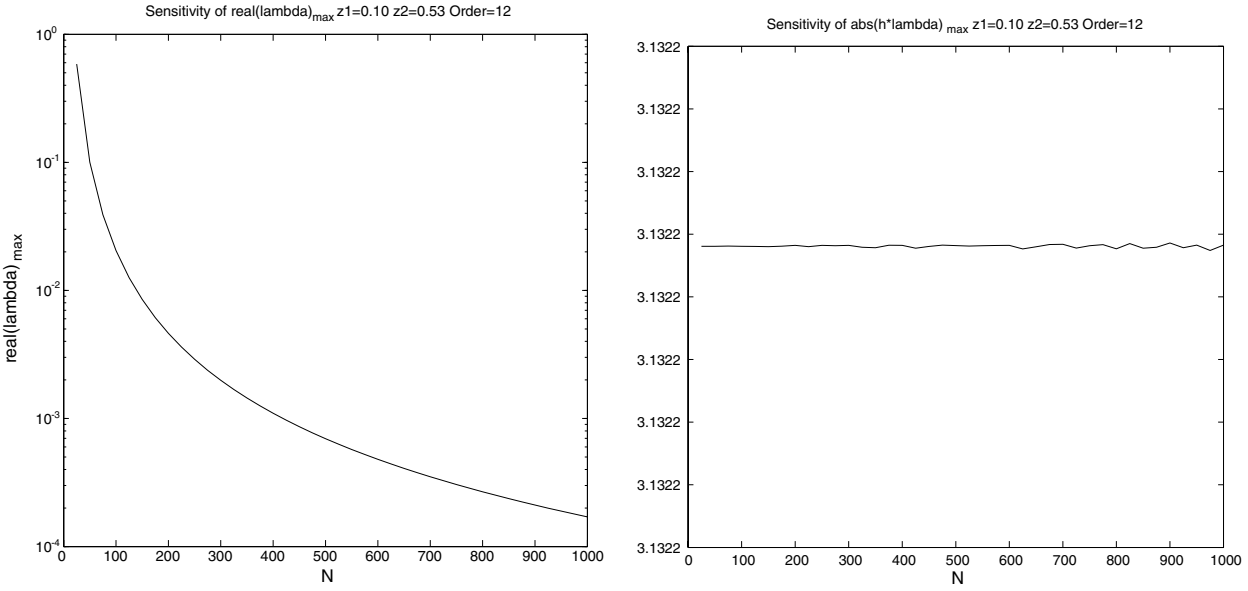

Fig. 7. Sensitivity of spectral quantities for $h\mathscr{D}_{12,h}$ with $p = 2$ and varying N.

3. Normal mode analysis

To further study the stability of the boundary closures derived above we carry out a normal mode analysis of the associated semidiscretized half-space problems. As discussed in [6, Chapter 12], this analysis leads to a problem of bounding the Kreiss determinant, which we now describe.

The half-space grid we consider is simply the union of the uniform grid with nonnegative integer nodes with the set of p extra nodes, z_j. We consider two transformed semidiscretized problems on this grid: the outflow problem

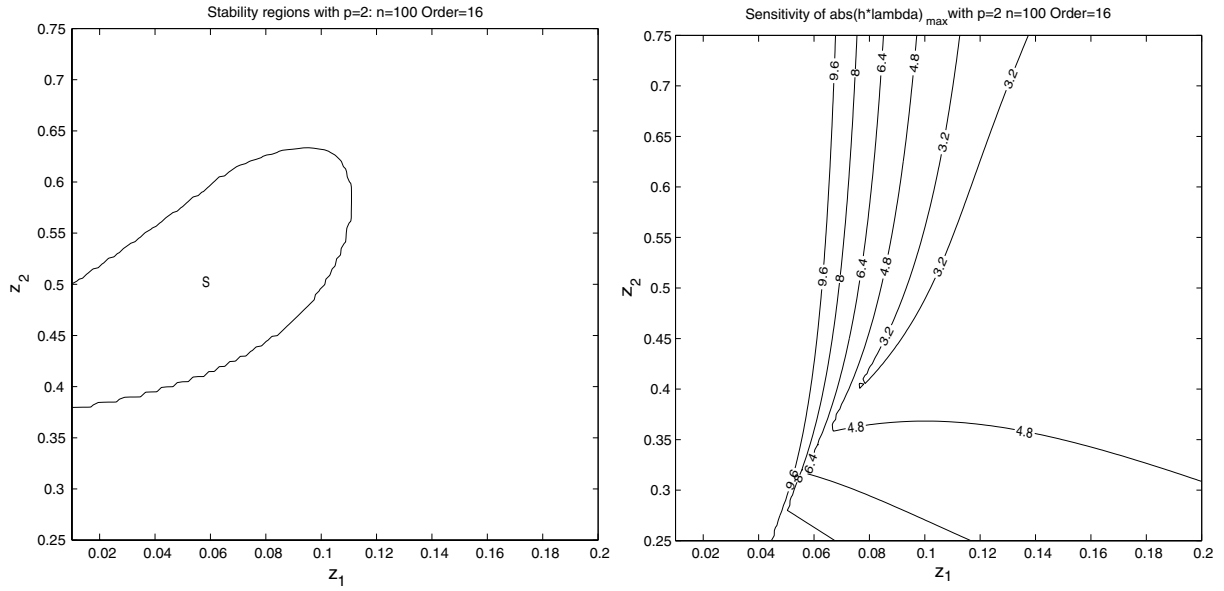

Fig. 8. Sensitivity of spectral quantities for $h\mathscr{D}_{16,h}$ with $p = 2$ and varying (z_1, z_2).

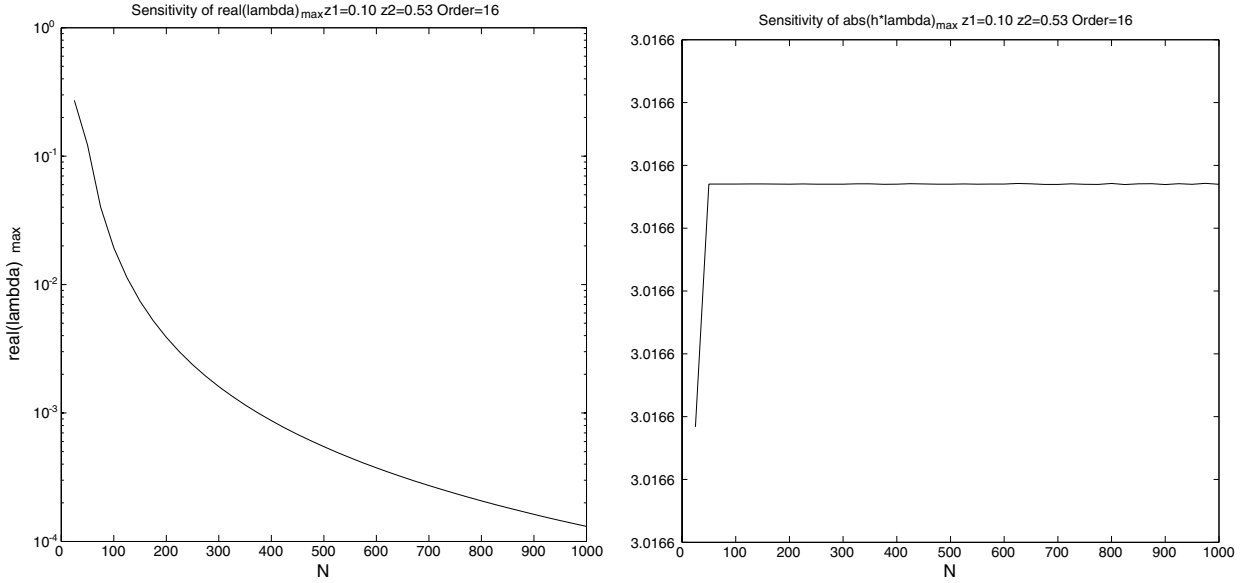

Fig. 9. Sensitivity of spectral quantities for $h\mathscr{D}_{16,h}$ with $p = 2$ and varying N.

$$s\hat{v} = \mathscr{D}_{2q,1}\hat{v}, \tag{3.7}$$

and the inflow problem

$$s\hat{v} = -\mathscr{D}_{2q,1}\hat{v},\ \hat{v}_0 = 0, \tag{3.8}$$

where $\hat{v}$ is an infinite grid vector. Taking $\Re s > 0$ we know that bounded solutions on the uniform grid are described by linear combinations of q modes:

$$\hat{v}_j = \sum_{v=1}^{q} \hat{c}_v \kappa_v^j,\ j > j_L, \tag{3.9}$$

where j_L is the index of the last nonintegral node z_p and where the functions $\kappa_v(s)$ represent the q independent roots of the characteristic equation for the order $2q$ central difference formula (2.2):

$$s\kappa^q \mp \sum_{k=1}^{q} \beta_k(\kappa^{q+k} - \kappa^{q-k}) = 0, \tag{3.10}$$

satisfying:

$$|\kappa_v(s)| < 1, \quad v = 1, \ldots, q. \tag{3.11}$$

(The existence of q roots inside the unit circle for $\Re s > 0$ follows from the symmetry of the central difference formula and the fact that roots satisfying $|\kappa| = 1$ can only exist for imaginary s.) Using (3.9) bounded solutions of (3.7) are determined by $\hat{v}_j$, $j = 0, \ldots, j_L + q$ and those of (3.8) by $\hat{v}_j$, $j = 1, \ldots, j_L + q$. Precisely, by solving (3.9) for the coefficients $\hat{c}_v$ given $\hat{v}_{j_L+1}, \ldots, \hat{v}_{j_L+q}$ we derive a representation in each case:

$$\begin{pmatrix} \hat{v}_{j_L+q+1} \\ \vdots \\ \hat{v}_{j_L+2q} \end{pmatrix} = X^{(\mathrm{in,out})}(s) \begin{pmatrix} \hat{v}_{j_L+1} \\ \vdots \\ \hat{v}_{j_L+q} \end{pmatrix}. \tag{3.12}$$

Using (3.12) in (3.7) we obtain a system of $j_L + q + 1$ equations parameterized by s:

$$H^{(\mathrm{out})}(s) \begin{pmatrix} \hat{v}_0 \\ \vdots \\ \hat{v}_{j_L+q} \end{pmatrix} = 0, \tag{3.13}$$

and similarly from (3.8) we obtain a system of $j_L + q$ equations:

$$H^{(\mathrm{in})}(s) \begin{pmatrix} \hat{v}_1 \\ \vdots \\ \hat{v}_{j_L+q} \end{pmatrix} = 0. \tag{3.14}$$

Necessary conditions for stability, the Godunov–Ryaben'kii conditions, are that these systems have no solutions for $\Re s > 0$. This is equivalent to the determinant conditions:

$$\det(H^{(\mathrm{in,out})}) \neq 0, \ \Re s > 0. \tag{3.15}$$

A sufficient condition for stability, on the other hand, is that the determinants are nonzero for $\Re s \geqslant 0$.

To check (3.15) numerically we have attempted to compute minimizers of the determinant in the region $\epsilon \leqslant \Re s \leqslant R_1$, $0 \leqslant \Im s \leqslant R_2$. The restriction to a bounded region can be justified by arguments given in [6, Chapter 12]. We have not, however, derived a precise estimate for R_1 or R_2. In our examples, we have chosen $R_1 = 20$ and $R_2 = 50$ which we believe to be sufficiently large; in particular the determinants are found to be large at the outer boundaries of the domain. Similarly we have chosen $\epsilon = 10^{-8}$ without a full theoretical justification.

The solutions of the actual minimization problems were computed using MATLAB's built-in minimization routines [12]. The results were found to be highly sensitive to the initial guesses or intervals prescribed. Therefore, we made a number of runs with different choices for these, but we cannot with certainty claim that all the global minima were found. Nonetheless, our results are completely consistent with the constructions based on the spectra. For all cases tested, including orders higher than the stability limits obtained above, the determinants were bounded below by $O(1)$ or greater constants at outflow. At inflow, on the other hand, $O(1)$ minima were found only for the cases for which the spectral analysis predicted stability; methods of order up through 8 for $p = 1$, up through 16 for $p = 2$, and up through 22 for $p = 3$. For higher order methods the minima found were at least five orders of magnitude smaller. In Table 2, we list the minimum values for the appropriately scaled determinant found by applying the minimization routine to cells of the form $x_j \leqslant \Re s \leqslant x_j + \frac{1}{5}$, $y_k \leqslant \Im s \leqslant y_k + \frac{1}{5}$, covering the region of interest.

Table 2
Minima of the Kreiss determinant

p	$2q$	$\det(H^{(\mathrm{out})})$	$\det(H^{(\mathrm{in})})$
1	6	2.4(0)	1.9(0)
1	8	6.0(0)	1.4(0)
1	10	1.5(1)	2.5(−7)
1	12	3.9(1)	4.6(−7)
2	8	4.4(0)	1.9(1)
2	10	1.3(1)	1.8(1)
2	12	3.6(1)	1.6(1)
2	14	1.0(2)	2.8(1)
2	16	2.9(2)	6.0(0)
2	18	7.8(2)	1.2(−5)
2	20	2.1(3)	7.2(−6)
3	16	2.5(2)	1.4(2)
3	18	8.2(2)	1.2(2)
3	20	2.5(3)	9.4(1)
3	22	6.5(3)	7.3(1)
3	24	1.4(4)	5.3(−5)
3	26	2.8(4)	4.7(−4)

Not unexpectedly, then, we find that the discretization of incoming characteristics, where we are in fact using a downwind procedure, is responsible for the observed stability limits. This analysis, though not definitive due to the difficulties in solving the determinant minimization problem, strongly bolsters our claim that the boundary closures are stable.

4. Dissipation operators

As is well-known the addition of artificial dissipation (or low-pass filtering) can enhance the performance and stability of difference methods for hyperbolic systems. Here we investigate the perturbations to the spectra induced by the addition of multiples of the natural dissipation operator associated with a $2q$th order approximation, namely an approximation to the $2q$th derivative using the same stencil. Precisely we consider:

$$\mathscr{D}_{2q,h} + (-1)^{q+1}\gamma h^{2q-1}\Xi_h \mathscr{D}_h^{2q}, \tag{4.16}$$

where γ is a positive parameter and $\mathscr{D}_h^{2q}$ is the matrix representing the approximation to the $2q$th derivative on the stencil defining $\mathscr{D}_{2q,h}$. The coefficients in this approximation follow simply from computing the $2q$th derivative of the degree $2q$ interpolating polynomial constructed on the stencil. Here Ξ_h is a cutoff function; a diagonal matrix whose diagonal elements are one except in the first and last r elements. These we have chosen to be zero, though less drastic cutoffs could also be tried.

Without the cutoff the dissipation operators had the defect that the resulting approximations were unstable for γ greater than some maximum value. Considering the continuous case, we note that the integral

$$\int u \frac{\mathrm{d}^{2q}u}{\mathrm{d}x^{2q}}\mathrm{d}x \tag{4.17}$$

is semidefinite only if the boundary terms vanish on integration by parts; that is only if appropriate boundary conditions are satisfied. On the other hand, if $\xi(x)$ is a nonnegative smooth cutoff function vanishing to high enough order at the boundaries, then

$$\int u \frac{\mathrm{d}^q}{\mathrm{d}x^q}\left(\xi \frac{\mathrm{d}^q u}{\mathrm{d}x^q}\right)\mathrm{d}x \tag{4.18}$$

obviously is semidefinite. Our matrix Ξ_h can be thought of as a crude representation of such a function. In our experiments, we have had success with this approach choosing $r = j_L + q + 1$ where $j_L + 1$ is the first point on the regular grid to the right of all the z_k. Then:

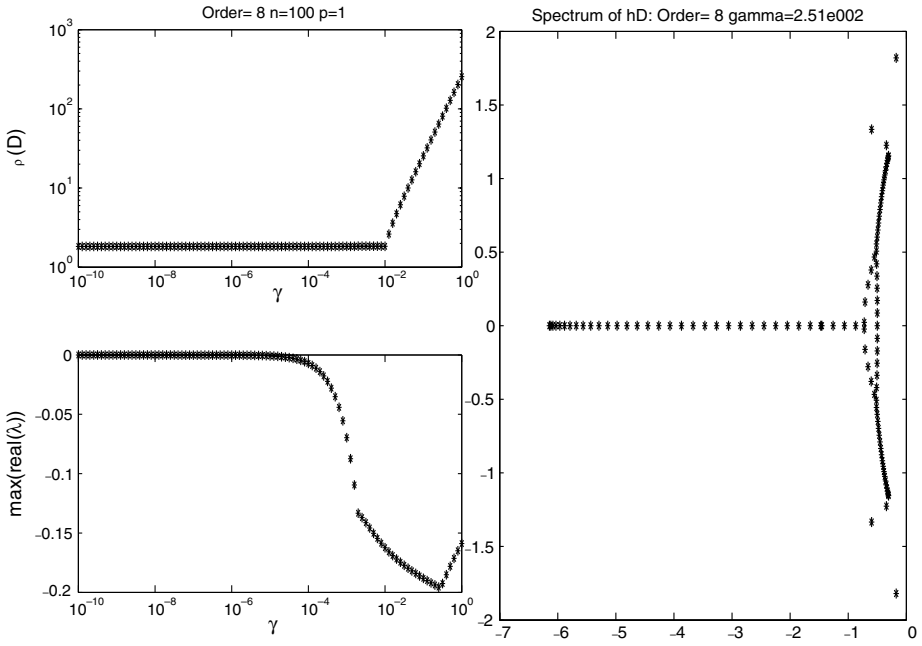

Fig. 10. Effects of dissipation for $p = 1$, $2q = 8$.

$$\mathscr{D}_h^{2q} = (D_+ D_-)^q, \tag{4.19}$$

the standard central difference dissipation operator.

A potential defect with the dissipation operators presented here is their asymmetry. We note that an alternative construction of symmetric artificial dissipation operators in the SBP context has been proposed in [14].

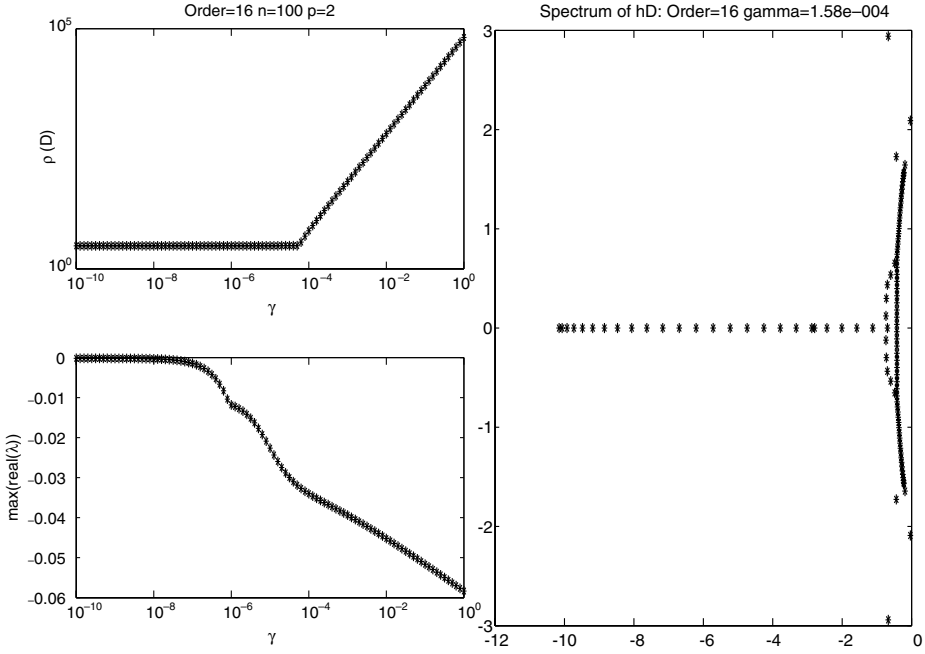

Fig. 11. Effects of dissipation for $p = 2$, $2q = 16$.

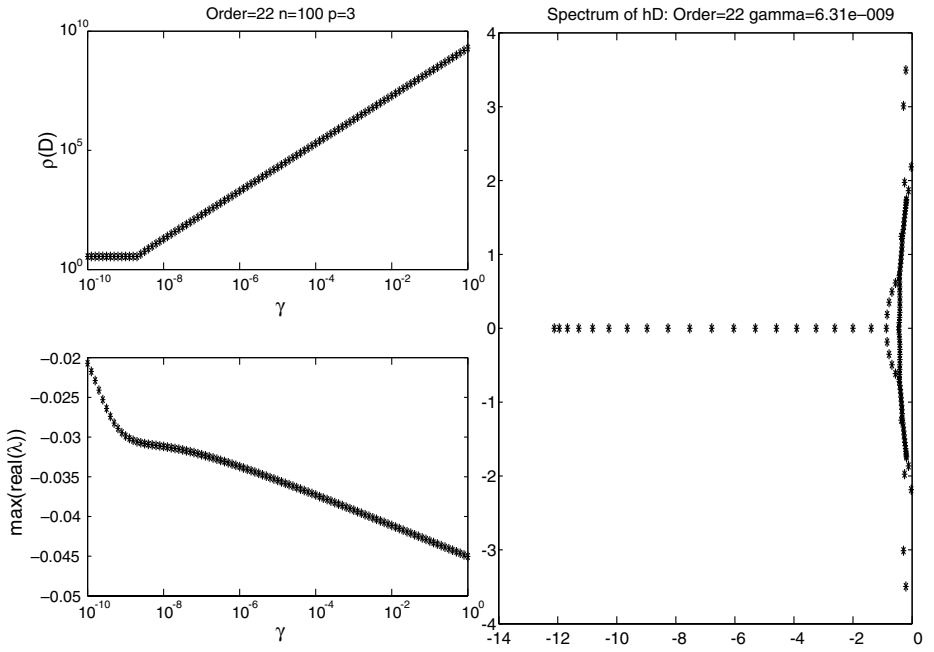

Fig. 12. Effects of dissipation for $p = 3$, $2q = 22$.

The idea is to use $h^{2q}\mathscr{D}_{q,h}^{T}B(h)\mathscr{D}_{q,h}$ where the weight matrix, B, is diminished near the boundaries to compensate for the fact that $\mathscr{D}_{q,h}^{T}$ is not a consistent derivative approximation; B is obviously related to our cutoff function. It may be of interest to pursue such a construction in our case. Nonetheless, we find that our straightforward approach leads to effective operators in some cases.

We consider the three maximal order methods discussed above: 8th order with $p = 1$, 16th order with $p = 2$, and 22nd order with $p = 3$. In each case we set $r = j_L + q + 1$. These are representative of all stable methods tested. Plotted in Figs. 10, 11 are the maximum real part of the eigenvalues of $h\mathscr{D}_{2q,h} + (-1)^{q+1}\gamma h^{2q}\Xi_h\mathscr{D}_h^{2q}$ with $N = 100$ and a logarithmically scaled sampling of γ. We also plot the spectrum for γ chosen from the sample to be the largest value for which the spectral radius is less than four times as large as the spectral radius of the unperturbed operator; in practice we would prefer to use smaller values of γ, and we typically do so in the numerical experiments.

The graphs of the spectral parameters in all cases are similar. For γ small the additional terms have no discernible effect. At some value of γ we observe a rapid decay of the maximum real part of the spectrum, and soon thereafter the spectral radius displays an even more rapid increase (Recall we are plotting the spectrum of $h\mathscr{D}$ so that in fact the decay rates are considerable.). Because of the rapid rise of the spectral radius, the effective range of the dissipation parameter is limited. Moreover, this range is quite different for each of the cases considered. From Fig. 10 we see that $10^{-5} < \gamma < 10^{-2}$ is suggested for $2q = 8$. For $2q = 16$, on the other hand, we conclude from Fig. 11 that the restriction $10^{-7} < \gamma < 10^{-4}$ is reasonable. Lastly, from Fig. 12 we suggest the range $10^{-10} < \gamma < 10^{-9}$ when $2q = 22$ (Smaller values of γ than tested here may also be useful for $2q = 22$.).

5. Extensions to optimized schemes

An important alternative to high-order, wide-stencil difference approximations to $\mathrm{d}/\mathrm{d}x$ are wide-stencil approximations which sacrifice order of accuracy to achieve good accuracy for a wider range of wavenumbers. Examples of this approach include the compact schemes proposed by Lele [13] as well as explicit, least-squares optimized formulas proposed by Tam and Webb [20] and Bogey and Bailly [2]. Here we follow the construction of [20], repeating the optimal grid construction given above for schemes of maximal order.

Precisely, Tam and Webb's dispersion relation preserving (DRP) schemes in the interior follow from minimizing the L_2 error in the dispersion relation over the interval $|kh| \leqslant \frac{\pi}{2}$ subject to the constraint of fourth order accuracy (The latter condition may be expressed as the exactness of the approximate derivative operator when applied to elements of Π^4, the vector space of fourth degree polynomials.). Precisely they solve the following minimization problem specialized to a uniform grid and a symmetric $2q+1$-point stencil:

Problem 2. For fixed h and $2q+1$-point stencil choose the coefficients of the difference operator, $\mathscr{D}^{\mathrm{DRP}}_{2q,h}$, to minimize

$$\int_{|k|h\leqslant\frac{\pi}{2}} |\mathscr{D}^{\mathrm{DRP}}_{2q,h} e^{ikx} - ike^{ikx}|^2 dk,$$

subject to the constraint

$$\mathscr{D}^{\mathrm{DRP}}_{2q,h} w(x) = \frac{dw}{dx}(x) \quad \forall w \in \Pi^4.$$

Obviously, on the uniform grids considered in [20] the factor e^{ikx} is superfluous as it is an eigenfunction of $\mathscr{D}^{\mathrm{DRP}}_{2q,h}$. This simplification is not applicable on the nonuniform boundary grids considered here. We now simply solve Problem 1 with $\mathscr{D}_{2q,h}$ replaced by $\mathscr{D}^{\mathrm{DRP}}_{2q,h}$ as defined at an arbitrary grid point and for an arbitrary stencil by the solution Problem 2. Note that we use the interior value of h to define the range of integration.

Numerically, we use the same brute force search as described above, solving Problem 2 directly via the introduction of Lagrange multipliers. The results, displayed in Table 3, are remarkably similar to those

Table 3
Optimized grid locations and spectra of $\mathscr{D}^{\mathrm{DRP}}_{2q,h}$

z_1	z_2	$2q$	N	$N^{-1}\rho(\mathscr{D})$	$N^{-1}\max_{\lambda\in\sigma(\mathscr{D})}\Re\lambda$
0.22	–	6	100	1.72	−1.14(−4)
0.19	–	8	100	1.89	−2.02(−4)
0.18	–	10	100	2.07	−2.16(−4)
0.14	0.99	10	100	2.85	−2.64(−4)
0.14	0.99	12	100	2.89	−3.24(−4)
0.13	0.94	14	100	2.92	−4.32(−4)
0.13	0.87	16	100	3.05	−7.58(−4)

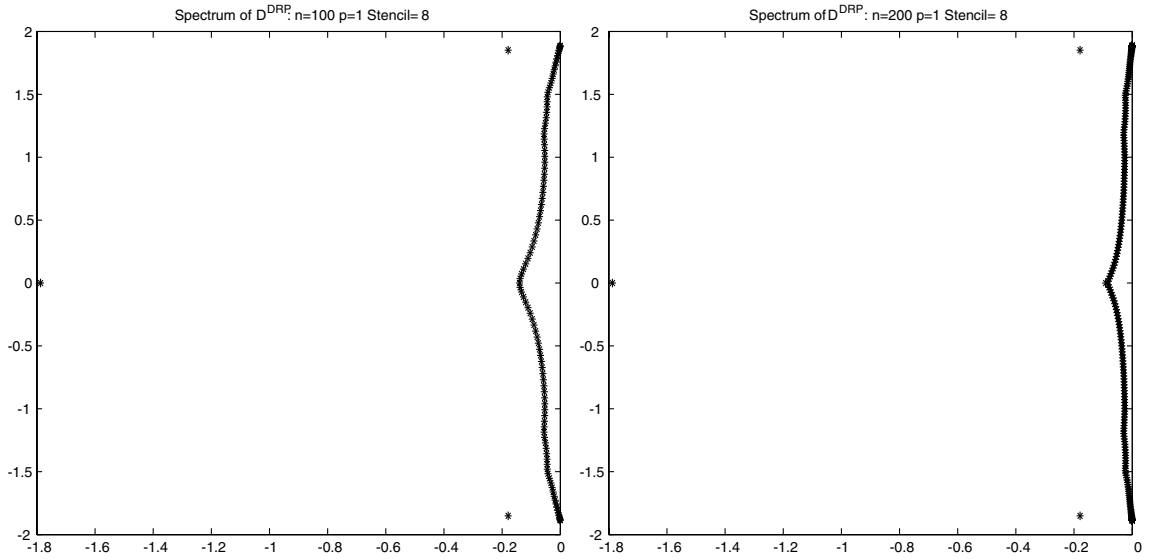

Fig. 13. Spectra of $h\mathscr{D}^{\mathrm{DRP}}_{8,h}$ for $p=1$.

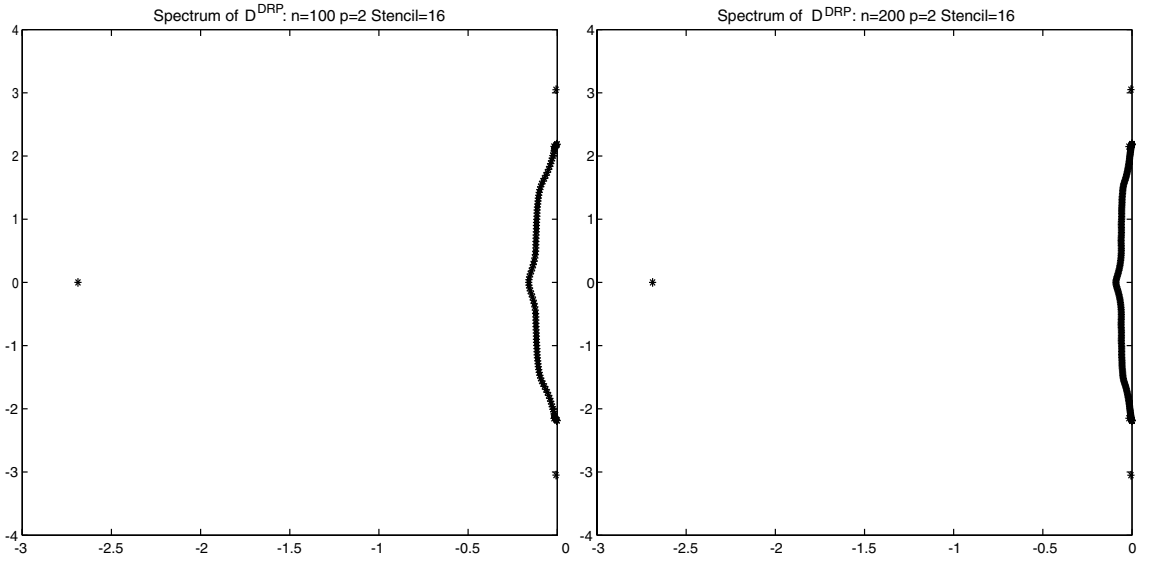

Fig. 14. Spectra of $h\mathscr{D}_{16,h}^{\mathrm{DRP}}$ for $p = 2$.

obtained for the maximal order schemes in terms of node location. However, it was possible to stabilize the $2q = 10$ DRP method with $p = 1$ which was not possible for the 10th order formula.

We also plot the spectra. Again the similarity between the graphs in Figs. 13, 14 and those in Figs. 1, 2 are striking. The main discernible differences are the kinks in the curve containing most of the DRP matrices' eigenvalues.

We have not carried out the normal mode stability analysis for these methods, though in principle it should be straightforward. Optimized dissipation operators or filters are also constructed in [2]. We have not included these in our analysis.

6. Numerical examples

In this section, we present three numerical examples to illustrate the theoretical results and to examine the relative performance of methods of differing order and with or without dissipation. In all cases time-stepping is accomplished by the standard fourth order Runge–Kutta method with relatively small time steps. In the first example, we consider the simple scalar system (2.3) with both smooth and discontinuous initial data. In the second case, we solve Maxwell's equations in a cavity with perfectly conducting walls. In the third, we solve the Euler equations linearized about a slightly subsonic Couette flow with wall boundary conditions on two sides and a perfectly matched layer (PML) on the others. In the first and second cases, we present results obtained with the three methods of maximal order: 8th order with $p = 1$, 16th order with $p = 2$, and 22nd order with $p = 3$. However, in the third case, where we have variable coefficients, we use slightly lower order methods, $2q = 12$, 18 for $p = 2$, 3, which were more favorable. See also [10] for additional experiments.

6.1. Convection of a pulse

We consider (2.3) with $F = 0$ and two initial conditions scaled to satisfy $\| g\|_{L_2} = 1$:

$$g(x) = \frac{8}{\sqrt{\pi}} \mathrm{e}^{-512\left(x-\frac{3}{4}\right)^2}, \quad g(x) = \begin{cases} 2, & \frac{3}{4} \leqslant x < 1, \\ 0, & 0 < x < \frac{3}{4} \end{cases} \tag{6.20}$$

Obviously in each case the exact solution will have propagated through the domain after $t = 1$. In the first, the pulse, though narrow, is smooth, while in the second case it is discontinuous. Of course we do not expect the high-order central schemes to do a good job of accurately representing the discontinuous solution; there will be a strong Gibbs phenomenon. However, we include it to test the stability of the boundary treatments under extreme circumstances and to verify that they do not lead to spurious reflections of unresolved waves.

We display results for the three maximal order closures using $N = 200$ and $\Delta t = \frac{1}{500}$. In Fig. 15, we plot the L_2-norm of the computed solution up to $t = 100$. For the smooth data we observe a precipitous drop in the norm as the pulse leaves the domain. For the discontinuous data the drop is not as rapid, however the solution does eventually become quite small. Plotting the solutions themselves we see that the phenom-

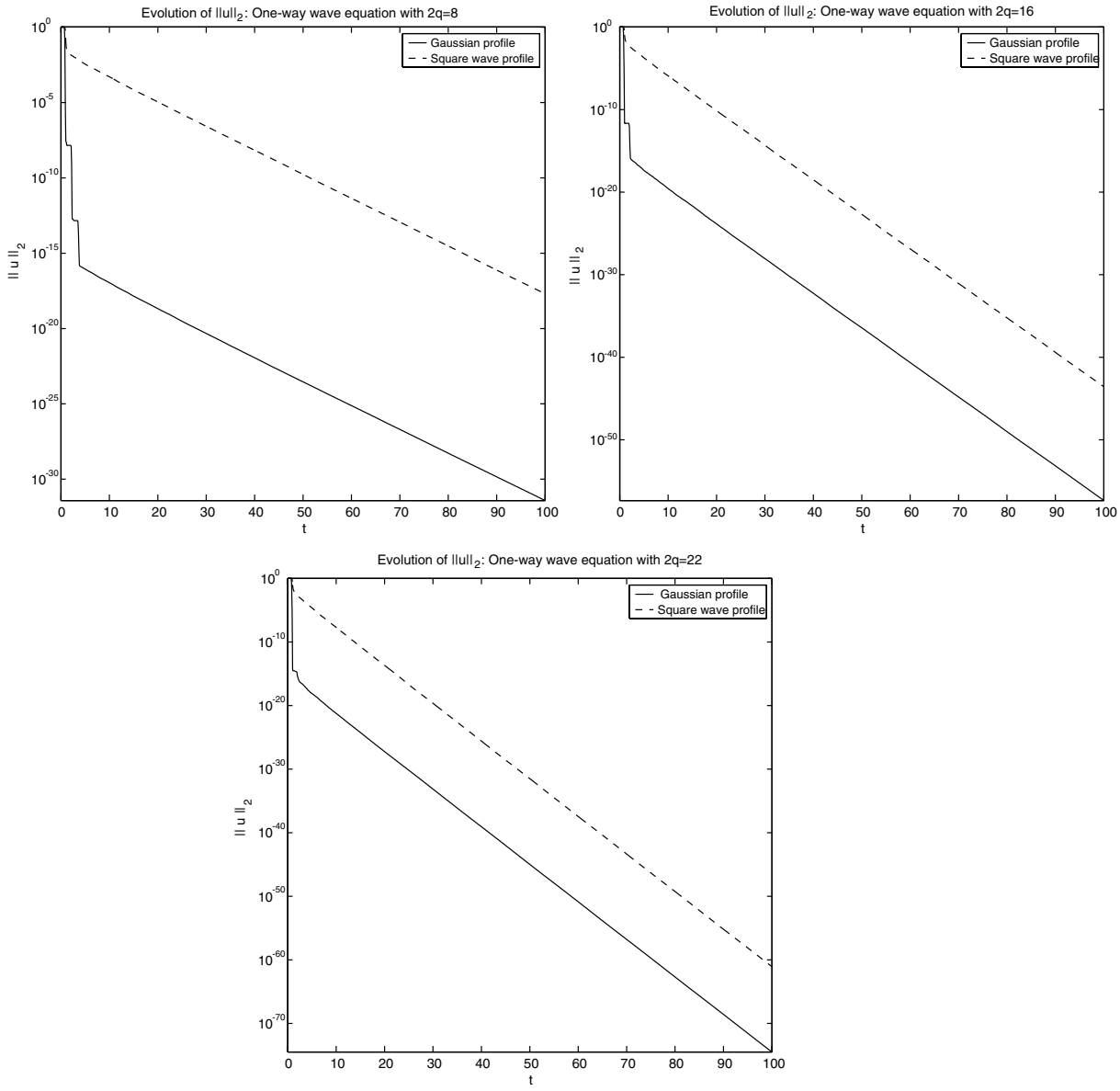

Fig. 15. Decay of solutions for the pulse propagation problem.

enon of slower decay in the nonsmooth case is not due to the boundary treatment. It is simply caused by the slow propagation speeds of the unresolved waves for the interior central difference approximations. The unresolved waves do not reflect. See Figs. 16–18.

6.2. TM modes in a cavity

We consider Maxwell's equations for TM modes in a cavity with perfectly conducting walls:

$$\frac{\partial E_z}{\partial t} = \frac{\partial H_y}{\partial x} - \frac{\partial H_x}{\partial y}, \quad \frac{\partial H_x}{\partial t} = -\frac{\partial E_z}{\partial y}, \quad \frac{\partial H_y}{\partial t} = \frac{\partial E_z}{\partial x}, \tag{6.21}$$

posed in $(x,y) \in [0,1]\times[0,1]$, $t \geqslant 0$, with $E_z = 0$ on the boundaries. We semidiscretize the system by:

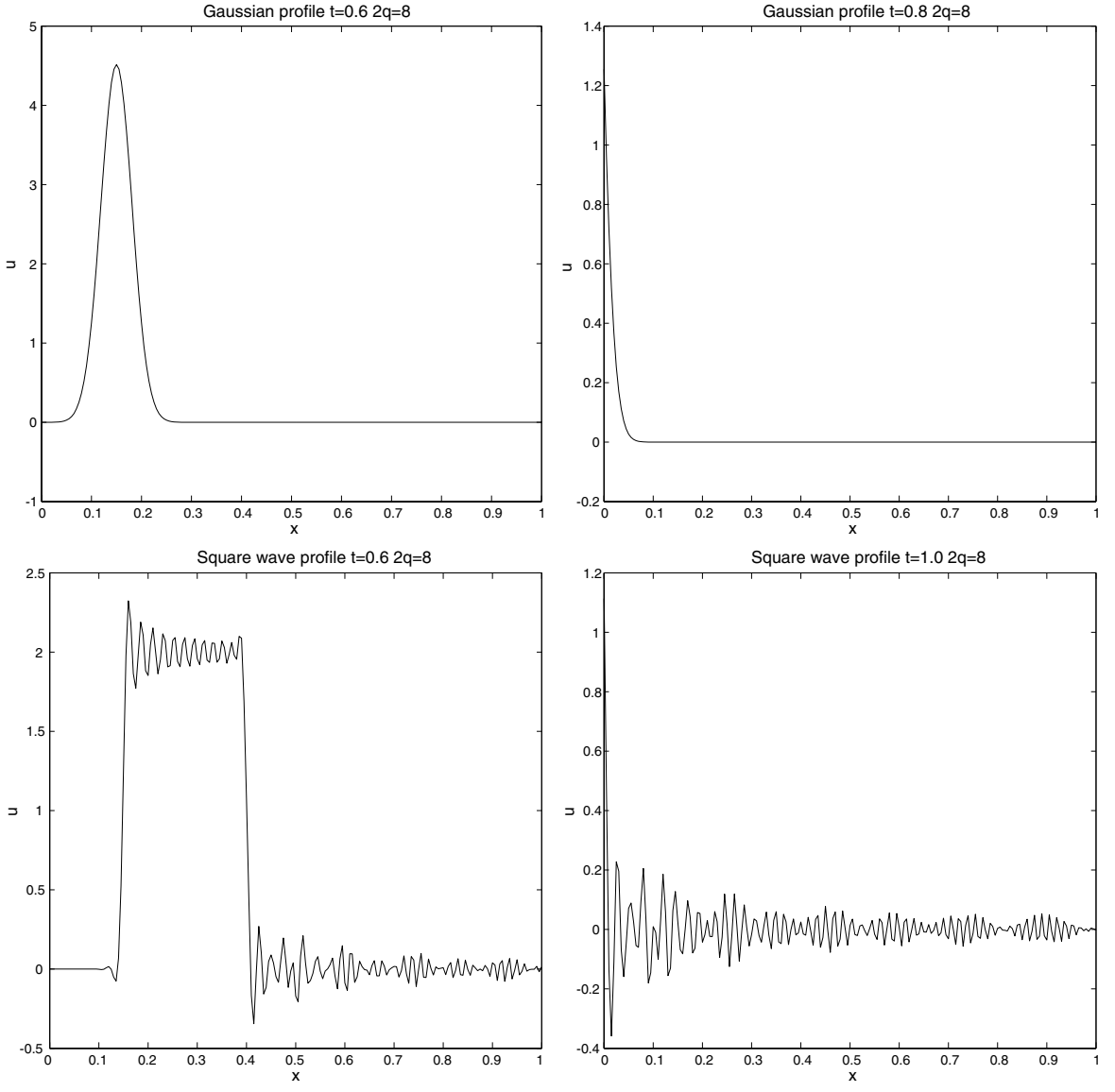

Fig. 16. Solutions of the pulse propagation problem with $2q = 8$.

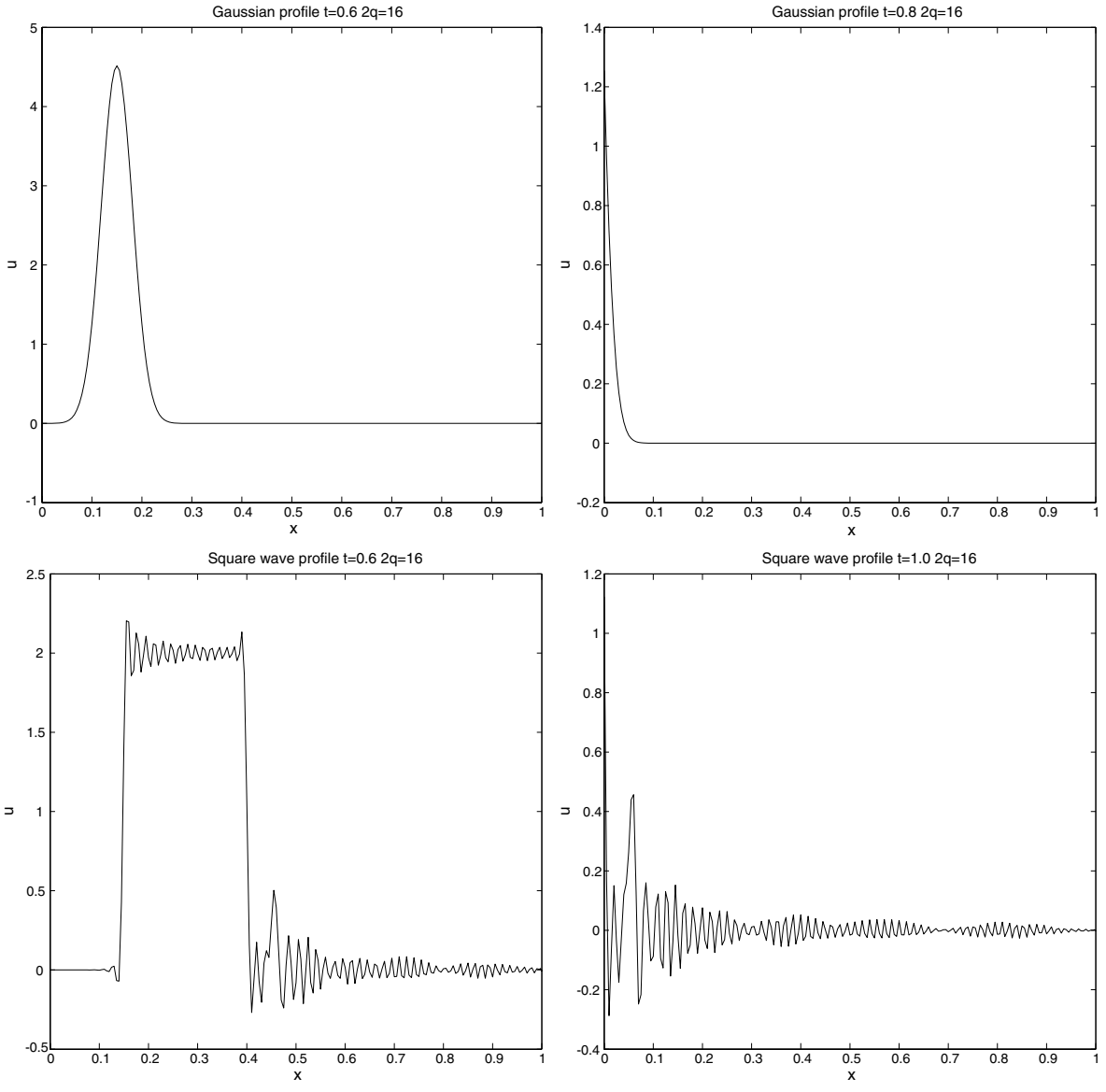

Fig. 17. Solutions of the pulse propagation problem with $2q = 16$.

$$
\begin{aligned}
\frac{\partial \tilde{E}_z}{\partial t} &= \mathscr{D}_{2q,h,x}\tilde{H}_y - \mathscr{D}_{2q,h,y}\tilde{H}_x + (-1)^{q+1}\gamma h^{2q-1}\left(\Xi_{h,x}\mathscr{D}_{h,x}^{2q} + \Xi_{h,y}\mathscr{D}_{h,y}^{2q}\right)\tilde{E}_z,\\
\frac{\partial \tilde{H}_x}{\partial t} &= -\mathscr{D}_{2q,h,y}\tilde{E}_z + (-1)^{q+1}\gamma h^{2q-1}\left(\Xi_{h,x}\mathscr{D}_{h,x}^{2q} + \Xi_{h,y}\mathscr{D}_{h,y}^{2q}\right)\tilde{H}_x,\\
\frac{\partial \tilde{H}_y}{\partial t} &= \mathscr{D}_{2q,h,x}\tilde{E}_z + (-1)^{q+1}\gamma h^{2q-1}\left(\Xi_{h,x}\mathscr{D}_{h,x}^{2q} + \Xi_{h,y}\mathscr{D}_{h,y}^{2q}\right)\tilde{H}_y.
\end{aligned}
\tag{6.22}
$$

The boundary conditions are imposed by computing the time derivatives of outgoing normal characteristic variables using linear combinations of (6.22) and one-sided differencing as discussed above and combining these with the equation $\tilde{E}_z = 0$.

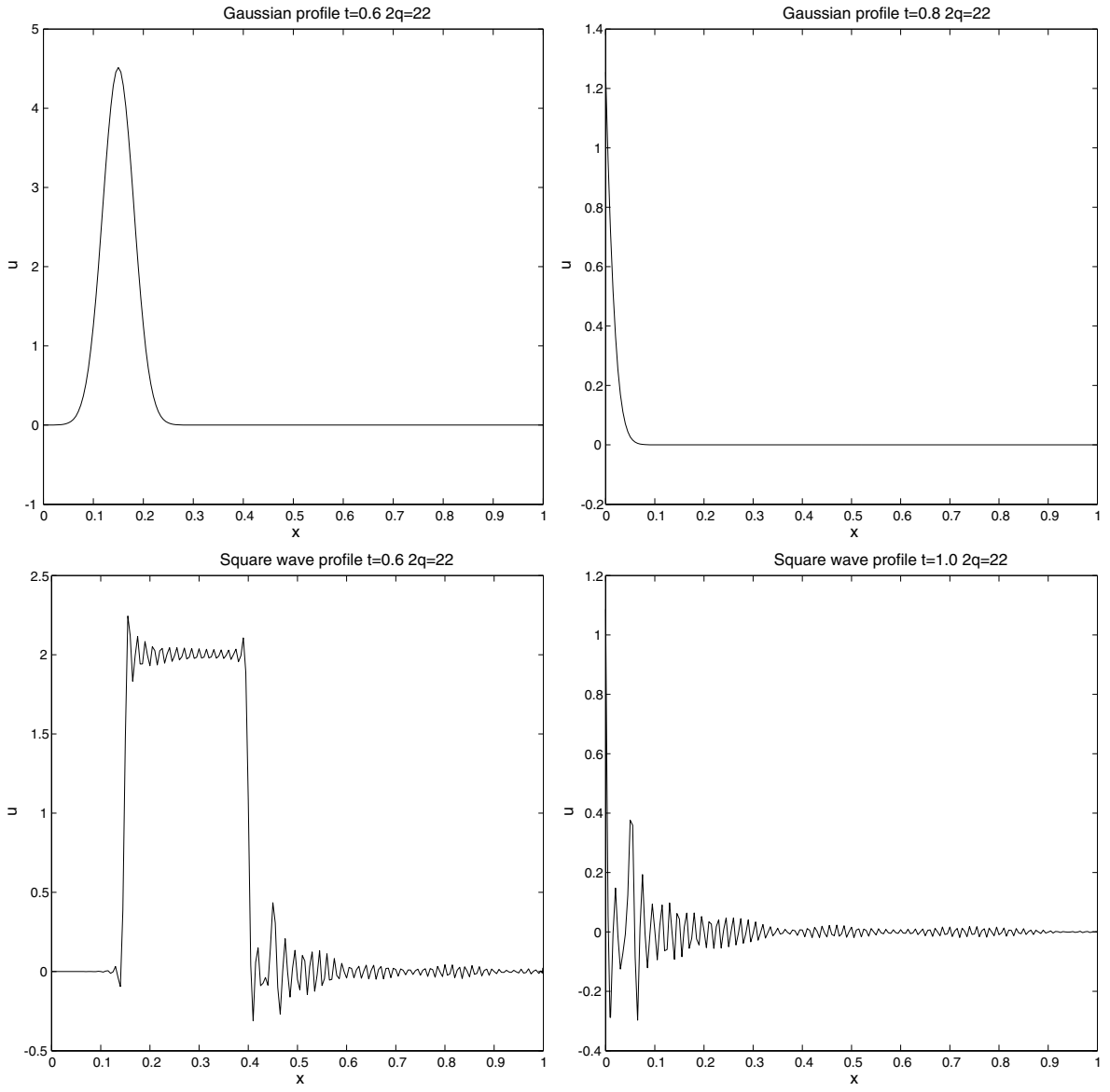

Fig. 18. Solutions of the pulse propagation problem with $2q = 22$.

We first study the accuracy of the methods by computing the solution:

$$\begin{aligned} E_z &= \sin 24\pi x \cdot \sin 27\pi y \cdot \cos 3\sqrt{145}\pi t, \\ H_x &= -\frac{9}{\sqrt{145}} \sin 24\pi x \cdot \cos 27\pi y \cdot \sin 3\sqrt{145}\pi t, \\ H_y &= \frac{8}{\sqrt{145}} \cos 24\pi x \cdot \sin 27\pi y \cdot \sin 3\sqrt{145}\pi t, \end{aligned} \tag{6.23}$$

for $0 \leqslant t \leqslant 100$. Note that this is more than 1800 periods. In Fig. 19, we plot the approximate L_2 errors in E_z for the twelve cases described in Table 4.

First of all, we note that the solutions are stable and accurate over the time intervals considered. For the 8th and 16th order methods there is a clear loss in accuracy when the artificial dissipation is included, though this effect could easily have been avoided by choosing smaller values of γ. For the 22nd order method the dissipation parameter was chosen so small that it had little effect on the error levels. We measured the observed

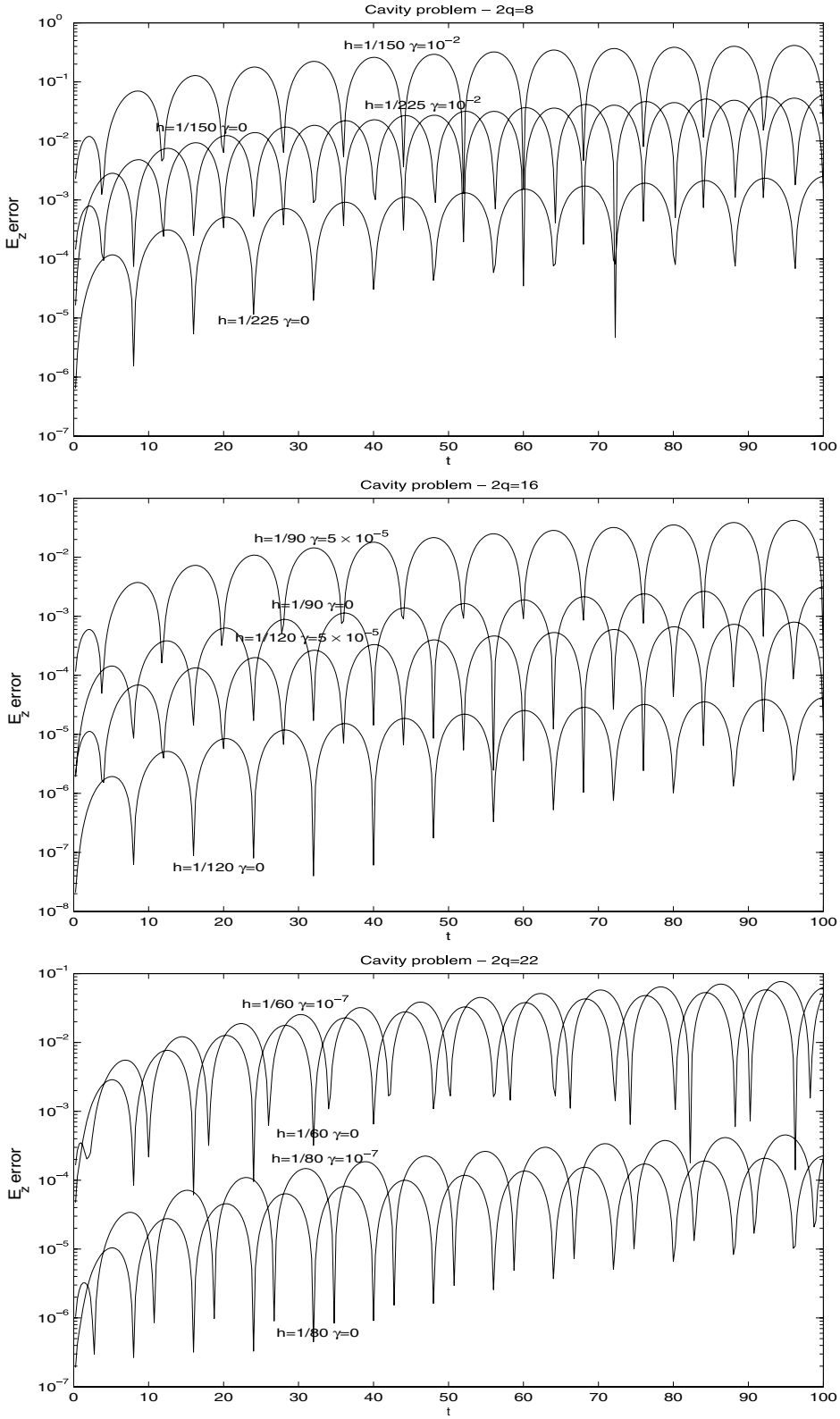

Fig. 19. Errors for the TM cavity mode problem.

Table 4
Cavity mode experiments

$2q$	p	γ	$h_x = h_y$	Δt
8	1	0	$\frac{1}{150}$	$\frac{1}{2432}$
8	1	0	$\frac{1}{225}$	$\frac{1}{5472}$
8	1	1E(−2)	$\frac{1}{150}$	$\frac{1}{2432}$
8	1	1E(−2)	$\frac{1}{225}$	$\frac{1}{5472}$
16	2	0	$\frac{1}{90}$	$\frac{1}{4860}$
16	2	0	$\frac{1}{120}$	$\frac{1}{15,360}$
16	2	5E(−5)	$\frac{1}{90}$	$\frac{1}{4860}$
16	2	5E(−5)	$\frac{1}{90}$	$\frac{1}{15,360}$
22	3	0	$\frac{1}{60}$	$\frac{1}{11,520}$
22	3	0	$\frac{1}{80}$	$\frac{1}{56,600}$
22	3	1E(−7)	$\frac{1}{60}$	$\frac{1}{11,520}$
22	3	1E(−7)	$\frac{1}{80}$	$\frac{1}{56,600}$

Table 5
Observed convergence rates

$2q$	p	γ	Average order
8	1	0	7.9
8	1	1E(−2)	5.5
16	2	0	15.0
16	2	5E(−5)	13.8
22	3	0	19.6
22	3	1E(−7)	17.9

convergence rate by looking at the ratios of the logarithms of the l_2-errors in space and time. This yields values consistent with the design accuracy, though slightly below. See Table 5.

Lastly, as the exact spatial operator with boundary conditions has purely imaginary eigenvalues, one might expect that the nondissipative methods are asymptotically unstable. That is, as the eigenvalues of the discrete problem are not structurally forced to be purely imaginary, we have no a priori reason to expect that they will not have small real parts of either sign (This will not be an issue for boundary conditions which are not everywhere perfectly reflecting.). This possibility for long time growth for a conservative problem does in fact occur. Setting $h_x = h_y = \frac{1}{30}$ we solved with less oscillatory data up to $t = 10^4$, measuring the error in time increments of 20. Growth in the error to $O(1)$ was observed for $\gamma = 0$ by $t = 1880$ for $2q = 8$, by $t = 2440$ for $2q = 16$, and by $t = 300$ for $2q = 22$. When the dissipation was included, however, methods of all three orders were accurate through $t = 10^4$, and we expect that they are asymptotically stable.

We emphasize, however, that even though they are not asymptotically stable, the dissipation-free methods were shown to be accurate over long time intervals, so that the addition of dissipation is only required in the very special case of a completely conservative wave system (no radiation out of the domain) and then only for very long time simulations.

6.3. Linearized subsonic Couette flow with a PML

Our third example is taken from the 4th CAA workshop on benchmark problems. We solve the compressible Euler equations linearized about a subsonic Couette flow:

$$\frac{\partial \rho}{\partial t} + My\frac{\partial \rho}{\partial x} + \frac{\partial u}{\partial x} + \frac{\partial v}{\partial y} = 0, \tag{6.24}$$

$$\frac{\partial u}{\partial t} + My\frac{\partial u}{\partial x} + Mv + \frac{\partial p}{\partial x} = 0, \tag{6.25}$$

$$\frac{\partial v}{\partial t} + My\frac{\partial v}{\partial x} + \frac{\partial p}{\partial y} = 0, \tag{6.26}$$

$$\frac{\partial p}{\partial t} + My\frac{\partial p}{\partial x} + \frac{\partial u}{\partial x} + \frac{\partial v}{\partial y} = 0, \tag{6.27}$$

with a reference Mach number of $M = 0.9$. Here the physical domain is given by $(x,y) \in (-2,2) \times (0,1)$, $0 \leqslant t \leqslant 64$, and at the top and bottom we impose the wall boundary condition, $v = 0$. Initial data, prescribed in [9], is given by a dipole pressure pulse plus an entropy pulse. We give its precise form in Appendix.

As in [10], we terminate the computational domain with perfectly matched layers to absorb outgoing waves (see also [8]). The modified equations in the PML are:

$$\frac{\partial \rho}{\partial t} + My\left(\frac{\partial \rho}{\partial x} + \sigma\mu\rho + \Psi_\rho\right) + \frac{\partial u}{\partial x} + \sigma\mu u + \Psi_u + \frac{\partial v}{\partial y} = 0, \tag{6.28}$$

$$\frac{\partial u}{\partial t} + My\left(\frac{\partial u}{\partial x} + \sigma\mu u + \Psi_u\right) + Mv + \frac{\partial p}{\partial x} + \sigma\mu p + \Psi_p = 0, \tag{6.29}$$

$$\frac{\partial v}{\partial t} + My\left(\frac{\partial v}{\partial x} + \sigma\mu v + \Psi_v\right) + \frac{\partial p}{\partial y} = 0, \tag{6.30}$$

$$\frac{\partial p}{\partial t} + My\left(\frac{\partial p}{\partial x} + \sigma\mu p + \Psi_p\right) + \frac{\partial u}{\partial x} + \sigma\mu u + \Psi_u + \frac{\partial v}{\partial y} = 0, \tag{6.31}$$

and for $w = \rho,\ u,\ v,\ p,\ \Psi_w = \psi_{1,w} + \psi_{2,w}$ and:

$$\frac{\partial \psi_{1,w}}{\partial t} + (\alpha + \sigma)\psi_{1,w} + \sigma\left(\frac{\partial w}{\partial x} + \sigma\mu w + \psi_{2,w}\right) = 0, \tag{6.32}$$

$$\frac{\partial \psi_{2,w}}{\partial t} + \alpha\psi_{2,w} + \sigma\mu\alpha w = 0. \tag{6.33}$$

The layer equations are solved in the domains $(-3.5, -2) \times (0,1)$ and $(2, 3.5) \times (0,1)$ with wall boundary conditions, $v = 0$, at the top and bottom and differentiated normal characteristic boundary conditions at the outer edges, $x = \pm 3.5$. Precisely, at $x = -3.5$, which is an inflow boundary, we set:

$$\frac{\partial}{\partial x}(\rho - p) = 0,\ \frac{\partial}{\partial x}(u + p) = 0,\ \frac{\partial v}{\partial x} = 0, \tag{6.34}$$

and at $x = 3.5$, which is an outflow boundary,

$$\frac{\partial}{\partial x}(u - p) = 0. \tag{6.35}$$

Here we use $\sigma_{\max}\tanh\eta|x - x_L|$ as our absorption profile with $x_L = \pm 2$ the interface location. With this choice the solution is expected to be continuously differentiable across the layer interface but no smoother. Thus we do not compute differences across the interface but rather solve in three domains independently, the physical domain and the two PMLs. At the interfaces after each time step we impose continuity by setting the normal characteristic variables from the left or right subdomain; that is we take the values of $\rho - p$, $u + p$ and v from the left and $u - p$ from the right. The precise values of the layer parameters in the experiments are:

$$\alpha = 0.5,\ \mu = 0.5,\ \sigma_{\max} = 20,\ \eta = 2. \tag{6.36}$$

The discretizations are as in the preceding example; first order space derivatives are approximated with $\mathscr{D}_{2q,h}$ in each subdomain and, when used, the dissipation operators are added to each evolution equation. In the layer, these are only added to the equations corresponding to the physical variables. The wall boundary conditions are discretized indirectly by imposing equivalent conditions on the space derivatives. Thus at the walls we set $\frac{\partial p}{\partial y} = 0$ and compute $\frac{\partial v}{\partial y} \pm \frac{\partial p}{\partial y}$ using the one-sided formulas according to which represents the outgoing normal characteristic variable. Similarly, at the layer edges, besides the imposition of the derivative boundary conditions on the incoming characteristic variables, we use the one-sided formulas to compute the derivatives of the outgoing variables.

This problem challenges the proposed high-order discretizations in a number of ways. First of all, the Couette flow leads to significant shearing of the initial pulses while the PML leads to rapid spatial damping as the disturbances enter the layer. Second, it tests their capability to perform in a multidomain setting where there is limited smoothness across the interface. Third, the absorption parameter increases rapidly and the layer equations themselves are marginally stable; in fact it is probable that they are not asymptotically stable [8].

We present results in a number of cases which are described in Table 6. The difficulties presented by this example led to some decrease in the orders we could stably use for certain values of p and on certain grids. For $p = 1$, the 8th order method appeared to exhibit late time instabilities when we used a very coarse grid; these were not evident for finer grids. The 16th order method with $p = 2$ needed the artificial dissipation operators to produce stable results over the prescribed time interval. Reducing the order to 12, however, the computations were stable even without dissipation. Finally, with $p = 3$ stable results were obtained using 18th order discretizations but not with the method of order 22.

We note that it is generally expected that some dissipation or filtering is needed for problems with variable coefficients or nonlinearities. Given the fact the continuous problem itself has marginal stability properties, we view these results, which show that the methods could be successfully used with no dissipation, to strongly attest to the robustness of the boundary closures. However, they do suggest that when using the higher order schemes one should avoid the maximum order which could be stabilized for a given choice of p. Thus, in the presence of variable coefficients, we suggest limiting the order to 12 with $p = 2$ and 18 when $p = 3$.

Errors, plotted in Fig. 20, are computed by comparison with the long domain solution of [9]. Thus they include the effects not only of discretization error but also the domain truncation error and the discretization error of the long domain solution itself. The problem is designed to challenge domain truncation methods, and even with a layer as thick as we are using here, the domain truncation errors dominate for long time. This is clear from the grid and method independence of the long time errors. Moreover, the long domain solution was computed using the 8th order method with $h_x = h_y = \frac{1}{128}$ and $\Delta t = \frac{1}{2000}$. Thus the error data shown for the higher order, fine grid solutions is suspect in that our calculations here are likely more accurate than the reference solution itself. Nonetheless, it is still of some interest to look at the error plots. Here we only plot the pressure differences; differences in the other fields are similar except that the density seemed somewhat more sensitive to the choice of artificial viscosity.

Looking at the early time errors, that is before the effects of the domain truncation become dominant, we clearly observe rapid convergence with grid refinement, though generally not at the design order. Addition of the artificial viscosity clearly reduced the early time accuracy for the 8th and 16th order methods, but had little effect when $2q = 18$. Again we emphasize that the reference solution is not sufficiently accurate to make the error data reliable enough to assess convergence order, and we mainly present this example to show that the methods are stable an accurate even in the presence of strong inhomogeneities and gradients.

Table 6
Couette flow experiments

Case	$2q$	p	γ	$h_x = h_y$	Δt
1	8	1	0	$\frac{1}{32}$	$\frac{1}{400}$
2	8	1	0	$\frac{1}{64}$	$\frac{1}{1500}$
3	8	1	0	$\frac{1}{96}$	$\frac{1}{3375}$
4	8	1	1E(−2)	$\frac{1}{64}$	$\frac{1}{1500}$
5	12	2	0	$\frac{1}{32}$	$\frac{1}{500}$
6	12	2	0	$\frac{1}{64}$	$\frac{1}{6000}$
7	12	2	0	$\frac{1}{96}$	$\frac{1}{12{,}000}$
8	16	2	1E(−4)	$\frac{1}{64}$	$\frac{1}{6000}$
9	18	3	0	$\frac{1}{32}$	$\frac{1}{500}$
10	18	3	0	$\frac{1}{64}$	$\frac{1}{7500}$
11	18	3	0	$\frac{1}{96}$	$\frac{1}{22{,}500}$
12	18	3	2E(−8)	$\frac{1}{64}$	$\frac{1}{7500}$

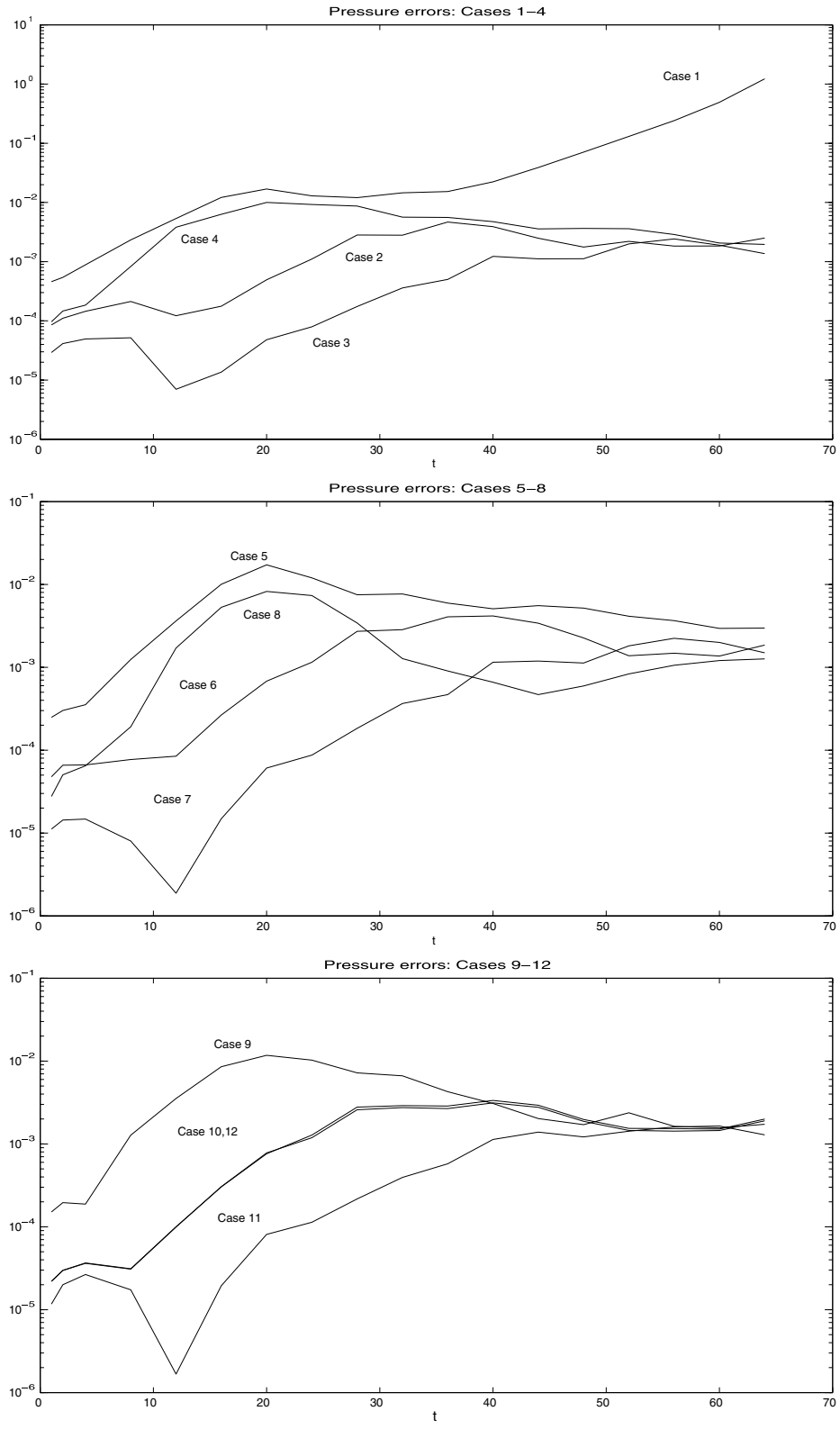

Fig. 20. Pressure differences with the solution in [9] for the Couette flow problem.

7. Conclusion

In summary, we have demonstrated that stable boundary closures for high-order central difference methods can be simply constructed via the introduction of a small number of additional grid points at judiciously chosen locations in the first one or two cells. These lead to effective methods of orders up to 22 for solving first-order linear hyperbolic systems. Beyond further testing, there are a number of extensions which seem worthy of consideration. These include:

i. Discretizations of the second derivative: we have, in fact, successfully tested 8th and 12th order two-step methods in space and time for the scalar wave equation using the grids constructed here; the idea is to compute approximations to powers of the Laplacian which appear in high-order temporal Taylor series. However, we have not systematically optimized the node locations.
ii. Development of improved dissipation operators; the ad hoc construction given here was only marginally useful.
iii. Stabilization of one-sided compact and staggered grid methods. As shown in [4] these have the potential for substantially better performance than the fixed grid explicit methods we have considered so far.

Acknowledgments

Supported in part by NSF Grants DMS-9971772 and DMS-0306285, ARO Grant DAAD19-03-1-0146, and Lawrence Livermore National Laboratory Subcontract B547968 Any conclusions or recommendations expressed in this paper are those of the author and do not necessarily reflect the views of NSF, ARO or LLNL.

Appendix A

A.1. Explicit formulas for 8th order closures

The 6×9 irregular block of $h\mathscr{D}_{8,h}$ near the left end of the grid $x_1, x_2 = x_1 + \frac{1}{5}h$, $x_j = x_1 + (j-2)h, j \geqslant 2$; that is, the coefficients for the approximate derivatives at the first six nodes.

$$\begin{pmatrix} -\frac{1063}{140} & \frac{1,953,125}{224,808} & -\frac{7}{4} & \frac{7}{6} & -\frac{5}{6} & \frac{35}{76} & -\frac{7}{40} & \frac{7}{174} & -\frac{1}{238} \\ -\frac{224,808}{78,125} & \frac{9,660,695}{4,720,968} & \frac{196,707}{156,250} & -\frac{524,552}{703,125} & \frac{56,202}{109,375} & -\frac{82,824}{296,875} & \frac{65,569}{625,000} & -\frac{54,264}{2,265,625} & \frac{3306}{1,328,125} \\ \frac{4}{7} & -\frac{1,953,125}{1,573,656} & -\frac{1}{5} & \frac{4}{3} & -\frac{5}{7} & \frac{20}{57} & -\frac{1}{8} & \frac{4}{145} & -\frac{1}{357} \\ -\frac{3}{14} & \frac{1,953,125}{4,720,968} & -\frac{3}{4} & -\frac{41}{180} & \frac{15}{14} & -\frac{15}{38} & \frac{1}{8} & -\frac{3}{116} & \frac{3}{1190} \\ \frac{2}{15} & -\frac{390,625}{1,573,656} & \frac{7}{20} & -\frac{14}{15} & \frac{3}{28} & \frac{14}{19} & -\frac{7}{40} & \frac{14}{435} & -\frac{1}{340} \\ -\frac{19}{140} & \frac{390,625}{1,573,656} & -\frac{19}{60} & \frac{19}{30} & -\frac{19}{14} & \frac{39}{76} & \frac{19}{40} & -\frac{19}{290} & \frac{19}{3570} \end{pmatrix} \tag{A.37}$$

A.2. Initial data for problem 2

$$p(x_1, x_2, 0) = P(x_1, x_2, 0), \tag{A.38}$$

$$P(x_1, x_2, t) = \sum_{i=1}^{2} B_i \sum_{k=-\infty}^{\infty} \int_{-\infty}^{t-r_{ik}} \frac{\mathrm{e}^{-\mu_i (s-\tau_i)^2}}{\sqrt{(t-s)^2 - r_{ik}^2}} \mathrm{d}s, \tag{A.39}$$

$$\rho(x_1, x_2, 0) = p(x_1, x_2, 0) + \sum_{k=-\infty}^{\infty} \mathrm{e}^{-\mu_S r_{Sk}^2}, \tag{A.40}$$

$$u(x_1, x_2, 0) = f_1(x_1) \int_{-2}^{2} \frac{\partial P}{\partial t}(z, x_2, 0) \mathrm{d}z - \int_{-2}^{x_1} \frac{\partial P}{\partial t}(z, x_2, 0) \mathrm{d}z, \tag{A.41}$$

$$v(x_1, x_2, 0) = -f_1\prime(x_1) \int_0^{x_2} \int_{-2}^{2} \frac{\partial P}{\partial t}(z, w, 0)\mathrm{d}z\,\mathrm{d}w. \tag{A.42}$$

where

$$r_{ik}^2 = (x_1 - x_{1,i})^2 + (x_2 - x_{2,ik})^2,\ r_{Sk}^2 = (x_1 - x_{1,S})^2 + (x_2 - x_{2,Sk})^2 \tag{A.43}$$

$$f_1(x_1) = \begin{cases} 0, & x_1 < -1.9 \\ 1 - \mathrm{e}^{-((x_1+1.9)/2.5)^8}, & |x_1| \leqslant 1.9 \\ 1, & x_1 > 1.9. \end{cases} \tag{A.44}$$

$$\tau_1 = \tau_2 = -.95,\ \mu_1 = \mu_2 = 30,\ B_2 = -B_1 = 1, \tag{A.45}$$

$$x_{1,1} = -x_{1,2} = 0.1,\ x_{2,10} = x_{2,20} = 1/2. \tag{A.46}$$

$$\mu_S = 12,\ x_{1,S} = 0,\ x_{2,S0} = 1/2. \tag{A.47}$$

$$x_{2,i,k+1} = 2 - x_{2,i,-k},\ x_{2,i,-(k+1)} = -x_{2,ik},\ k \geqslant 0, \tag{A.48}$$

$$x_{2,S,k+1} = 2 - x_{2,S,-k},\ x_{2,S,-(k+1)} = -x_{2,Sk},\ k \geqslant 0. \tag{A.49}$$

The parameters B_i, μ_i, $x_{1,i}$, $x_{2,ik}$, S, μ_S, $x_{1,S}$, $x_{2,Sk}$ are chosen so that, to a high degree of accuracy (11 digits), the initial data are supported on $(-2,2)$ and the boundary conditions are satisfied. The integrals are evaluated using a combination of Gaussian quadrature and endpoint corrected trapezoid rules, again to high accuracy.

References

[1] B. Alpert, Hybrid Gauss-trapezoidal rules, SIAM J. Sci. Comp. 20 (1999) 1551–1584.
[2] C. Bogey, C. Bailly, A family of low dispersive and low dissipative explicit schemes for flow and noise computations, J. Comput. Phys. 194 (2004) 194–214.
[3] M. Carpenter, D. Gottlieb, S. Abarbanel, Time-stable boundary conditions for difference schemes solving hyperbolic systems: methodology and application to high-order compact schemes, J. Comput. Phys. 111 (1994) 220–236.
[4] B. Fornberg, M. Ghrist, Spatial finite difference approximations for wave-type equations, SIAM J. Numer. Anal. 37 (1999) 105–130.
[5] B. Fornberg, D. Sloan, A review of pseudospectral methods for solving partial differential equations, Acta Numer. 3 (1994) 203–267.
[6] B. Gustafsson, H.-O. Kreiss, J. Oliger, Time-dependent Problems and Difference Methods, Wiley, New York, 1995.
[7] T. Hagstrom, Experiments with stable, high-order difference approximations to hyperbolic initial-boundary value problems, in: A. Bermudez, D. Gomez, C. Hazard, P. Joly, J. Roberts (Eds.), Proceedings of the Fifth International Conference on Mathematical and Numerical Aspects of Wave Propagation Phenomena, SIAM, Philadelphia, PA, 2000.
[8] T. Hagstrom, I., Nazarov, Perfectly matched layers and radiation boundary conditions for shear flow calculations. Technical Report 2003-3298, AIAA, 2003.
[9] T. Hagstrom, I. Nazarov, Exact solutions to category 1 problem 3, in: M. Dahl (Ed.), Proceedings of the Fourth CAA Workshop on Benchmark Problems, number CP-2004-21295, NASA, 2004, pp. 35–38.
[10] T. Hagstrom, I. Nazarov. Solution of category 1 benchmark problems using high-order difference methods and perfectly matched layers, in: M. Dahl (Ed.), Proceedings of the fourth CAA Workshop on Benchmark Problems, number CP-2004-21295, NASA, 2004, pp. 355–370.
[11] J. Hesthaven, T. Warburton, Nodal high-order methods on unstructured grids: I. Time-domain solution of Maxwell's equations, J. Comput. Phys. 181 (2002) 186–221.
[12] D. Higham, N. Higham, MATLAB Guide, SIAM, Philadelphia, 2005.
[13] S. Lele, Compact finite difference schemes with spectral-like resolution, J. Comput. Phys. 103 (1992) 16–42.
[14] K. Mattsson, M. Svärd, J. Nordström, Stable and accurate artificial dissipation, J. Sci. Comp. 21 (2004) 57–79.
[15] J. Nordström, M. Carpenter, High-order finite-difference methods, multidimensional linear problems, and curvilinear coordinates, J. Comput. Phys. 173 (2001) 149–174.
[16] P. Olsson, Summation by parts, projections and stability I, Math. Comp. 64 (1995) 1035–1065.
[17] P. Olsson, Summation by parts, projections and stability II, Math. Comp. 64 (1995) 1473–1493.
[18] B. Strand, Summation by parts for finite difference approximations for d/dx, J. Comput. Phys. 110 (1994) 47–67.
[19] M. Svärd, On coordinate transformations for summation-by-parts operators, J. Sci. Comp. 20 (2004) 29–42.
[20] C. Tam, J. Webb, Dispersion-relation-preserving finite difference schemes for computational acoustics, J. Comput. Phys. 107 (1993) 262–281.